Journal of African Earth Sciences 57 (2010) 79–95

Contents lists available at ScienceDirect

Journal of African Earth Sciences

journal homepage: www.elsevier.com/locate/jafrearsci

Nature, origin and significance of the Fomopéa Pan-African high-K calc-alkaline plutonic complex in the Central African fold belt (Cameroon)

Maurice Kwékam [a,*], Jean-Paul Liégeois [b], Emmanuel Njonfang [c], Pascal Affaton [d], Gerald Hartmann [e], Félix Tchoua [f]

[a] Département des Sciences de la Terre, Faculté des Sciences, Université de Dschang, B.P. 67 Dschang, Cameroon
[b] Département de Géologie, Musée Royal de l'Afrique Centrale, B-3080 Tervuren, Belgium
[c] Laboratoire de Géologie, Ecole Normale Supérieure, Université de Yaoundé I, B.P. 47, Yaoundé, Cameroon
[d] CEREGE, Aix-Marseille Université, CNRS, B.P. 80, Europôle méditerranéen de l'Arbois, 13545 Aix-en-Provence cedex 04, France
[e] Geowissenschaftliches Zentrum Göttingen, GZG, Abt. Geochemie, Universität Göttingen, Goldschmidtstraße 1, 37077 Göttingen, Germany
[f] Laboratoire de Géodynamique interne, Faculté des Sciences, Université de Yaoundé I, B.P. 812 Yaoundé, Cameroon

ARTICLE INFO

Article history:
Received 2 December 2008
Received in revised form 11 July 2009
Accepted 23 July 2009
Available online 3 August 2009

Keywords:
High-K calc-alkaline granitoids
Pan-African
Post-collision
Linear lithospheric delamination
Fomopéa

ABSTRACT

The Fomopéa plutonic complex in West Cameroon comprises three petrographical units: a biotite–hornblende granitoid (BHG) including some diorite, a biotite monzogranite (BmG) and an edenite syenogranite (EsG). Amphibolites occur within each unit. The massif was emplaced into a Pan-African amphibolite-facies metamorphic basement. All rocks display igneous textures and are chemically calc-alkaline, the BHG being metaluminous (ASI < 1) the BmG (ASI = 0.98–1.06) and EsG (ASI = 0.94–1.1) being metaluminous to weakly peraluminous. U–Pb dates on zircon give a Pan-African age of 620 ± 3 Ma for a diorite and 613 ± 2 Ma for a quartz–monzodiorite, both belonging to the BHG. Sr–Nd isotopic data indicate the mixing between a juvenile source, probably the mantle (nearest Fomopéa pole: $\varepsilon_{Nd(620\ Ma)} = +4$ and $^{87}Sr/^{86}Sr_{(620Ma)} = 0.703$) and a Palaeoproterozoic to Archaean lower continental crust (nearest Fomopéa pole: $\varepsilon_{Nd(620Ma)} = -16$ and $^{87}Sr/^{86}Sr_{(620Ma)} = 0.709$; Nd $T_{DM} = 2.9$ Ga) through a contamination process or through a bulk mixing event at the base of the crust. Evidence for both processes is provided by the coexistence of mafic enclaves and gneissic xenoliths within the granitoids. We propose a model whereby linear lithospheric delamination occurred along the Central Cameroon shear zone (CCSZ) in response to post-collisional transpression. This delamination event induced the partial melting of the mantle and old lower crust, and facilitated the ascent of the magmas. The emplacement of numerous post-collisional Neoproterozoic plutons along the CCSZ during the Pan-African orogeny indicates that this process was of paramount importance. The continental signature and geophysical data from the area indicate that the CCSZ corresponds to the northern lithospheric boundary of the Archaean Congo craton, and that the events recorded here correspond to the metacratonic evolution of the northern boundary of the Congo craton.

1. Introduction

The Neoproterozoic Pan-African belt of Cameroon is a part of the Central Africa Pan-African belt. It connects to the west with the coeval Trans-Saharan orogenic belt; to the south it is in contact with the Archaean Congo craton, and to the north it borders the Saharan metacraton (Abdelsalam et al., 2002). This belt is connected with the northeastern Borborema Province of Brazil, which is part of the Neoproterozoic Brasiliano belt (Almeida et al., 1981; Brito et al., 2002; Lerouge et al., 2006).

Early work on the Central Africa Pan-African fold belt focused mainly on the tectonic evolution of the belt, and the general aspects of magmatic activity associated with it (e.g. Tubosum, 1983; Nédélec et al., 1986; Toteu et al., 1987, 1990; Barbey et al., 1990; Affaton et al., 1991; Ekwueme et al., 1991; Ngako et al., 1991, 1992, 2003; Penaye et al., 1993; Ferré et al., 1998, 2002). After a structural synthesis of the Eastern Nigeria and Northern Cameroon belts, Ngako (1999) suggested a continent–continent collision for the area comparable to the Himalaya collision. This model supposes the existence of one Archaean block in the Sahara which moved from NNE to SSW about 630 Ma ago forming the Central African fold belt along the Archaean Congo craton. This block is now identified as the Saharan metacraton (Abdelsalam et al., 2002).

* Corresponding author. Tel.: +237 77516684.
E-mail addresses: mkwekam@yahoo.fr (M. Kwékam), jean-paul.liegeois@africamuseum.be (J.-P. Liégeois), affaton@cerege.fr (P. Affaton).

1464-343X/$ - see front matter © 2009 Elsevier Ltd. All rights reserved.
doi:10.1016/j.jafrearsci.2009.07.012

The Pan-African belt of Cameroon includes three structural domains separated by major shear zones (Zones 1, 2, 3 in Fig. 1): (1) the southern domain comprises Pan-African metasedimentary units, whose protoliths were deposited in a passive margin environment at the northern edge of the Congo craton; (2) the central domain includes Palaeoproterozoic metasediments and orthogneiss intruded by widespread syn- to late-tectonic granitoids mainly transitional in composition and of crustal origin (Soba et al., 1991; Tchouankoué, 1992; Ganwa, 1998; Tchakounté, 1999; Toteu et al., 2001) and having high-K calc-alkaline affinities (Kwékam, 1993; Talla, 1995; Nguiessi-Tchankam et al., 1997; Njonfang, 1998; Tagne-Kamga, 2003; Nzolang et al., 2003); (3) the Northern domain consists of the Poli series (Ngako, 1986; Njel, 1986; Toteu, 1990) that possesses the most oceanic character of the various Neoproterozoic basins present in Cameroon (Toteu et al., 2006a), Pan-African granitoids of mainly calc-alkaline composition emplaced between 660 and 580 Ma (Toteu et al., 1987, 2001), late alkaline granitoids and numerous basins made up of unmetamorphosed sedimentary and volcanic rocks.

Here we present the Fomopéa Pan-African magmatic complex, emplaced along the Central Cameroon Shear Zone (CCSZ) that separates the central from the northern domain (Fig. 1) as a large

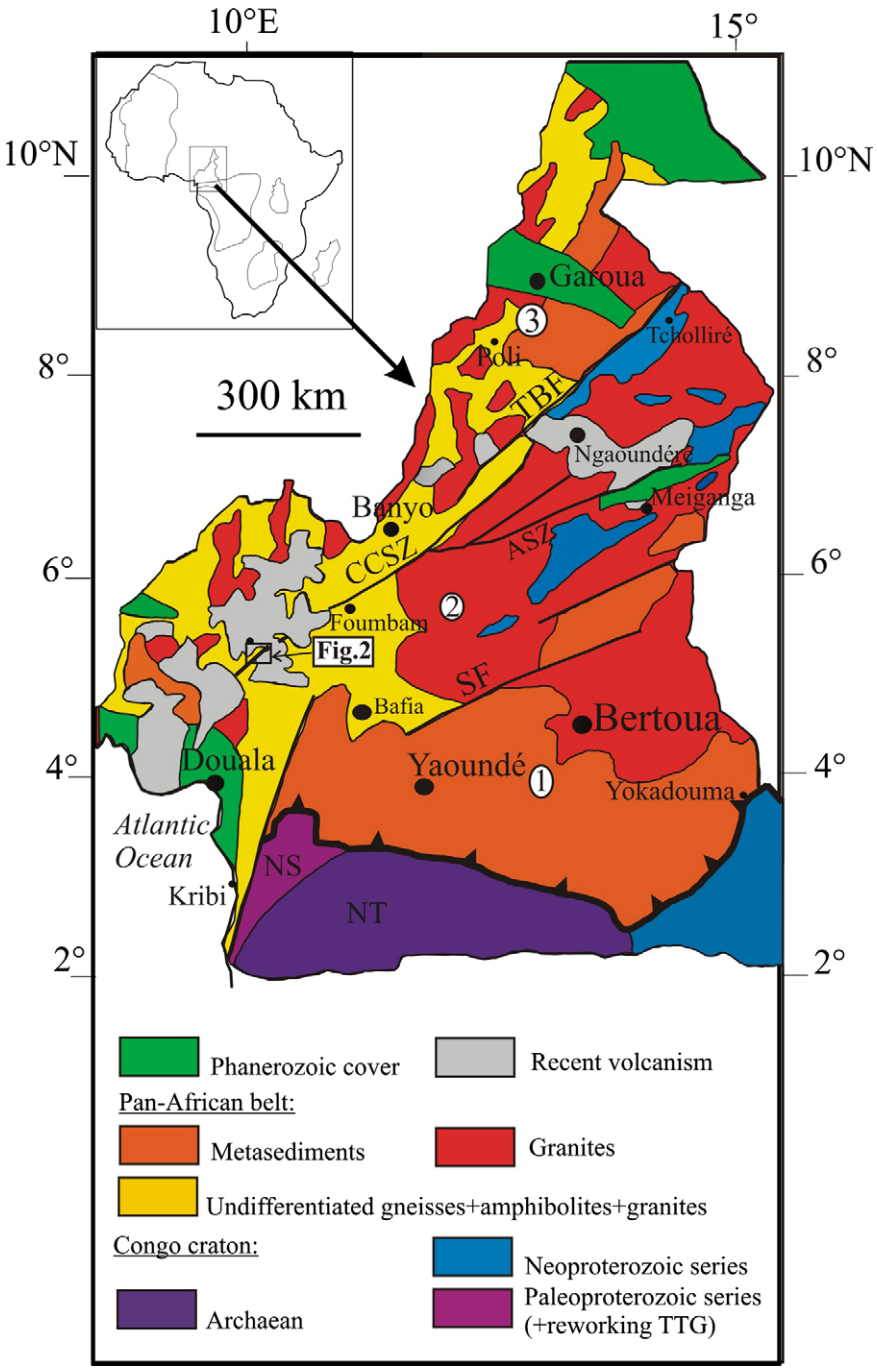

Fig. 1. Geological map of Cameroon, showing the major lithotectonic domains; ASZ, Adamawa shear zone; SF, Sanaga fault; TBF, Tcholliré-Banyo fault; CCSZ, Central Cameroon shear zone; NT, Ntem complex; DS, Dja group; NS, Nyong group; 1 = southern; 2 = central domain (Adamawa–Yadé domain of Toteu et al., 2004); 3 = northern domain.

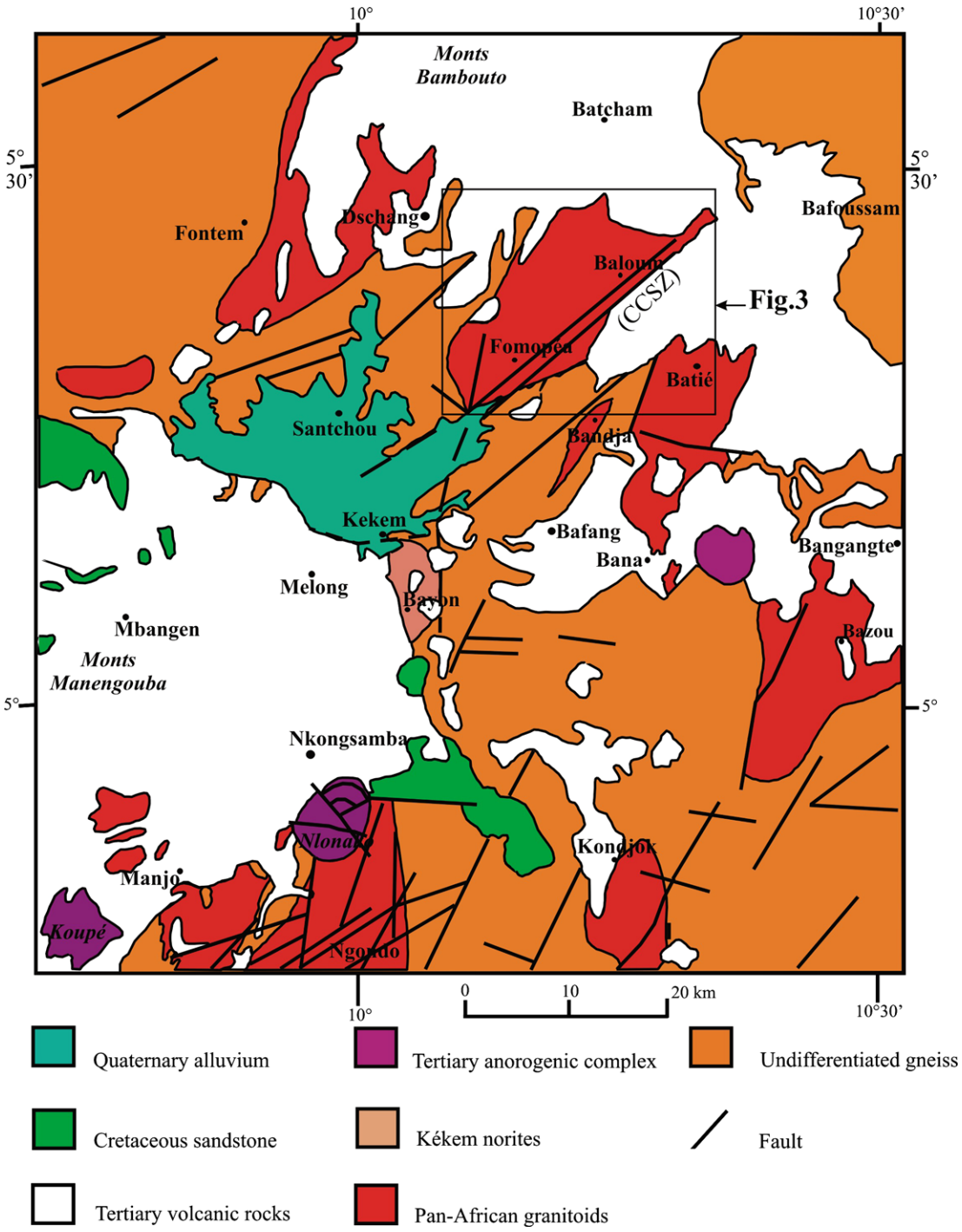

Fig. 2. Extract of West-Cameroon geological map from Dumort (1968) showing the locality of the Fomopéa plutonic complex and its neighbouring plutons (e.g. Batié, Ngondo, Bangangté, etc.).

number of similar Pan-African granitoids (Fig. 2). Cameroon Pan-African granitoids are mostly post-collisional and considered to have emplaced at around 580 Ma (Kwékam, 1993; Talla, 1995; Nguiessi-Tchankam et al., 1997) from a source of mixed origin (Tagne-Kamga, 2003) or made up of recycled old crustal material (Nzolang et al., 2003; Penaye et al., 2004; Nzolang, 2005; Kwékam, 2005). Based on field, petrographical, major, trace and Rb–Sr, Sm–Nd, U–Pb isotope data, this work attempts to define the nature, origin and age of the Fomopéa granitoids for constraining their geodynamic setting in the Pan-African belt of Cameroon, which knowledge is essential for deciphering West African geology, as Fomopéa is located between the West African craton, the Congo craton and the Saharan metacraton.

2. Structural setting

The Neoproterozoic Pan-African belt in West Cameroon comprises granito-gneissic units intruded by mafic to felsic plutons

(including the Fomopéa complex) and overlain by Cenozoic volcanic complexes.

Four Pan-African regional tectonic phases have been recognized in Cameroon (Toteu et al., 2004). The D_1 phase created a flat-lying foliation and would correspond to early Pan-African nappe tectonics, verging east. The D_2 deformation formed a foliation with steep axial planes and is associated with tight and upright folds and with syn-migmatitic conjugate shear zones; the D_2 deformation is considered to be the result of an E–W regional shortening direction inducing a NE–SW transcurrent movement. Both D_1 and D_2 phases are associated with a N110–140°E stretching lineation. The D_3 phase is related to sinistral movements along the N–S to NE–SW shear zones. The final D_4 phase is characterized by N80–110°E dextral and N160–180°E sinistral shear zones. The D_1–D_2 phase are continued to the 635–615 Ma age range, the D_3 to the 600–580 Ma age range and the D_4, poorly dated, is older than 545 Ma (Toteu et al., 2004, and references therein). These four phases, associated to collisional and post-collisional evolution in the Cameroon domain, have been more recently identified as corresponding to three successive tectonic events (Ngako et al., 2008): (1) crustal thickening (ca 630–620 Ma) including the thrusting (D_1) and shortening (D_2) of Toteu et al. (2004); (2) the left lateral wrench movements (613–585 Ma) among which the Sanaga Shear zone, corresponding to D_3 of Toteu et al. (2004); (3) the right lateral wrench movements (ca. 585–540 Ma) mainly marked by the Central Cameroon Shear Zone (CCSZ) and corresponding to D_4 of Toteu et al. (2004). The CCSZ is a 70°E striking major crustal structure extending from Sudan into NE Brazil. It defines a fan-geometry in central Cameroon, due to its interaction with N40°E directed shear zone system (Ngako et al., 2003). The CCSZ seems to have been initiated earlier than the D_4 phase, during the left lateral wrench movements, as indicated by sinistral shear sense indicators with the same movement direction (Ngako et al., 2003; Njonfang et al., 2006, 2008) compatible with successive shearing events, within the dextral shear zones. The tectonic evolution of the Pan-African belt in central and southern Cameroon is characterized by transpression, because of coeval shear and thrust kinematic interactions. The resulting structures include the N70°E sinistral shear zones of central Cameroon (CCSZ and Sanaga fault) and the granulitic and migmatitic thrust sheets overriding the Congo craton (Ngako et al., 2003).

In the Fomopéa area, the granito-gneiss country rocks are affected mainly by the shortening phase of crustal thickening. The schistosity and foliation planes are mainly oriented N110°E and are associated with folds and a stretching mineral lineation of the same orientation. They are often affected by N70°E ductile shear zones and are cut by N70°E migmatitic leucosomes corresponding to the second tectonic event. The magmatic fabrics (flowage) observed in the Fomopéa plutonic complex are oriented N–S to NNE–SSW (N0°–N30°E), parallel to the flow deformation found in the anatectic granite (e.g. Dschang granite) outcropping in the country-rocks. They dip towards E to ESE, in the opposite direction to that of the anatectic granite (towards NW), and are thus not parallel to the foliation of the gneissic country-rocks. However, the Fomopéa complex, like other neighbouring massifs, is elongated parallel to the regional foliation. This suggests that the geometry of the Fomopéa complex is linked to a late crustal thickening event and could be the result of the same regional stress in response to the contrasted rheological behaviour of the country rocks relatively to the moving Fomopéa magmas. The northern and northeastern edges of the massif are overlain by Cenozoic trachytic and basaltic lavas. Recent sedimentary rocks partially overlay its south-western edge, the remaining being blurred by the presence of post-magmatic dextral NE–SW faults associated with mylonite (Kwékam, 1993), probably related to the last tectonic event.

3. Field geology of the Fomopéa plutonic complex

The Fomopéa complex is made up of three main groups of plutonic rocks (Fig. 3): biotite–hornblende granitoids (BHG, including some dioritoids), a biotite monzogranite (BmG) and an edenite syenogranite (EsG). Small lens-shaped bodies, bands or masses with cumulus texture of amphibolitic rocks are often found in each group.

The BHG is located around Fomopéa village. The main rock types are a porphyritic monzogranite usually grey in colour, and a dark green quartz–monzodiorite; subordinate quartz–monzonite and equigranular granodiorite are also present. Spindle-shaped enclaves of diorite and angular xenoliths of gneissic rocks are frequently observed. These enclaves are commonly elongated parallel to the magmatic foliation, defined by the alignment of amphibole, biotite, platy feldspar and schlierens. Schuppen structures present in a granitic "proto-dyke" indicate a dextral strike-slip ductile fault oriented N100°E.

The BmG forms a large homogeneous body to the NE in the Baloum area but is also crosscutting dykes intruding the BHG. Microdioritic enclaves are common, particularly along the contact with the BHG.

The EsG forms a body located to the SE, around the Fontsa-Toula and Fotoufem villages. It contains small enclaves of diorite (<5 cm in diameter). The contact with the south-western border of the BHG is progressive and often blurred by amphibolite panels whereas the contact with the gneissic country rocks is sharp. The magmatic foliation is marked by the alignment of amphibole and rare schlierens of amphibole.

The magmatic foliation in the different petrographic groups is sub-parallel to the massif elongation (NNE–SSW dipping ESE) and the regional foliation, giving it a sheet-like structure and suggesting syn-kinematic emplacement. This magmatic foliation is observed throughout the BHG unit (N0–30°E) with dips varying from 50°ESE in the margin to 85°ESE in the core, and rather lower to the margins of the BmG (N0–10°E, N50–75° ESE or E) and EsG (N10–15°E, N30–50° ESE). However, features of a syn- to late-kinematic pluton relative to the late crustal thickening event are suggested by the alignments of the minerals, and enclaves of diorite and gneissic country rocks in the presence of schuppen structures. Indeed, the Fomopéa pluton can then be considered as an early post-collisional Pan-African pluton, older than the abundant syntectonic granitic plutons (Toteu et al., 2006a) of the second to third tectonic events. The whole massif is fringed on its NE–SW edge by amphibolite bands that are mainly oriented N40°E with a dip of 60° to the SE, and on its SE edge by N50°E dextral mylonitic band, and a few late dykes of microgabbro crosscut the Fomopéa pluton.

4. Petrography

The biotite–hornblende granitoids (BHG) include diorite, quartz–monzodiorite, quartz–monzonite, granodiorite and monzogranite. The rocks are medium- to coarse-grained, with biotite, hornblende, plagioclase, K-feldspar and quartz as the major mineral phases and magnetite, zircon, apatite, titanite and allanite as common accessory phases. The rocks display well-defined magmatic textures. Plagioclase is often zoned and has andesine composition (An_{50-35}). Green, brownish to reddish biotite (X_{Mg} = 0.45–55) is common. Hornblende, the main amphibole, occurs both as euhedral prisms and as anhedral crystals often surrounding euhedral flakes of biotite. Its chemical composition vary from tschermakitic hornblende (X_{Mg} = 0.50–0.60) in diorite to magnesio-hornblende (X_{Mg} = 0.54–0.56) in the BHG. Titanite, the most abundant accessory mineral, may reach more than 4% volume in some samples. Secondary minerals, chlorite, actinolite and epidote occur as subsolidus alteration products of biotite, hornblende and plagioclase.

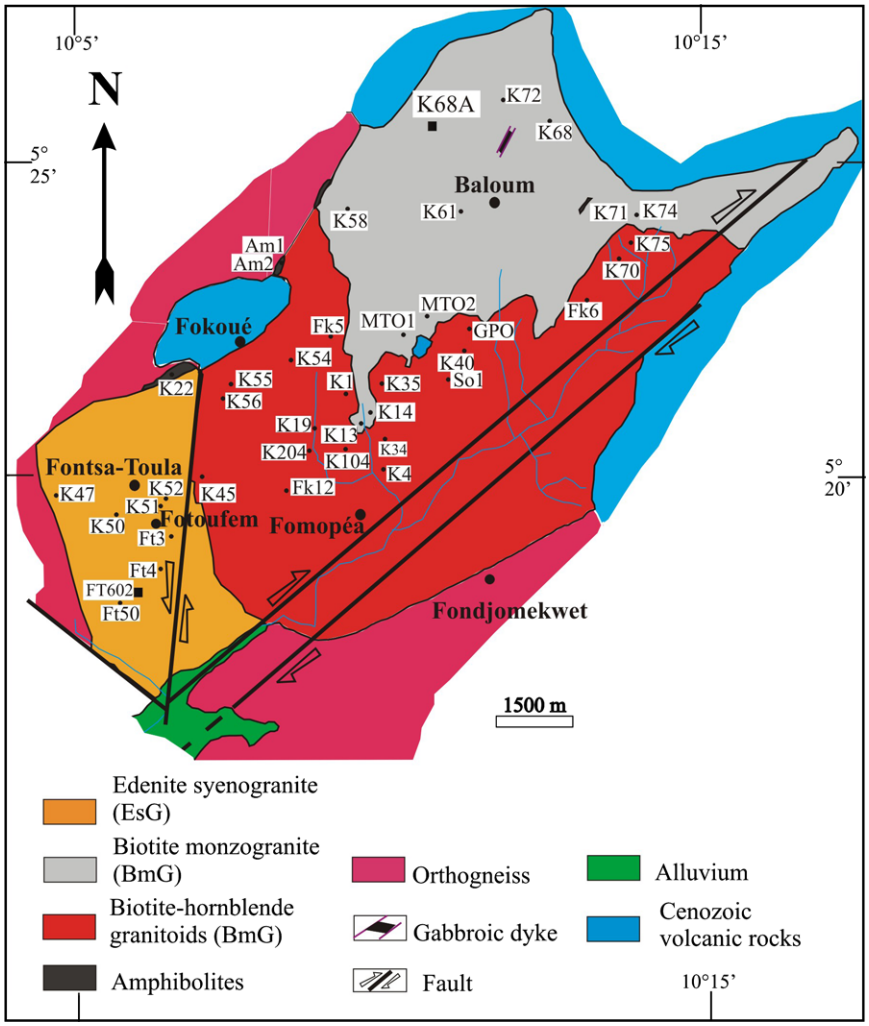

Fig. 3. Geological map of the Fomopéa plutonic complex.

The biotite–monzogranite (BmG) is fine- to medium-grained and heterogranular. The main mineral phases are brownish to reddish biotite (X_{Mg} = 0.45–0.50), zoned plagioclase (An_{25-30}), K-feldspar (microcline) and quartz whereas the accessory minerals remain the same as in the BHG except allanite which was not found. Secondary minerals are sericite and chlorite, resulting from the alteration of feldspar and biotite, respectively, while muscovite occurs as a hydrothermal mineral. Late magmatic to subsolidus deformation imprints such as undulose extinction in quartz grains, minor sub-grain development along quartz–quartz boundaries, mechanical twinning in feldspars and herringbone cleavage (kink-band) in biotite are common in this monzogranite.

The edenite–syenogranite (EsG) is leucocratic, medium-grained and heterogranular. It differs from the BmG mainly by the absence of biotite and the occurrence of amphibole. As a whole, it contains larger quartz crystals, K-feldspar, plagioclase (An_{5-25}, dominantly albite) and green sub-euhedral to euhedral hornblende (X_{Mg} = 0.50–0.70). Accessory minerals include titanite, apatite and Fe–Ti oxides. As in the BmG, undulose extinction in quartz grains and mechanical twinning in feldspars are observed.

The chemical compositions of biotite from the Fomopéa rocks plot in the calc-alkaline field of Nachit et al. (1985) in Kwékam (2005). The amphibole geothermobarometer of Johnson and Rutherford (1989) calculated for magmatic hornblende gives a temperature range of 710–760 °C with pressure varying from 2.2 to 4.8 kbar. Higher grade conditions are obtained in the diorite and lower ones in the edenite syenogranite.

5. U–Pb on zircon and Rb–Sr on whole-rock geochronology and Sr–Nd isotopes

5.1. Analytical techniques

U–Pb analytical data were obtained at the Isotopic Geochemistry Laboratory (IGL), University of Kansas, following the procedures described by Toteu et al. (1994). All zircons analyzed were air-abraded for 2–4 h to remove as much of the altered outermost part as possible (Krogh, 1982). All U–Pb analyses were performed on single grains; all our samples were spiked with ^{205}Pb–^{235}U tracer solution before dissolution. Results are given in Table 1.

Sr isotopes on whole rocks were measured at the Royal Museum for Central Africa, Tervuren (Belgium). After dissolution in an HF/$HClO_4$ mixture, Sr was separated on Dowex 50/150 ion exchange resin. Total chemical blanks range between 10 and 15 ng Sr. Measurements were carried out on a GV Sector 54 TIMS. An error of 4% on Rb/Sr ratios is estimated on standard and sample replicates. The external reproducibility on NBS987 standard solution was 0.710255 ± 0.000015 during the course of this study. Sr compositions were corrected to a value of 0.710250 for NBS987 and frac-

Table 1
U-Pb zircon data obtained on different fractions extracted from the dioritic sample K204 and quartz monzodioritic sample K104.

Sample	Isoplot data												Calculated ages					
	Fraction	Size (mg)	U (ppm)	Pb (ppm)	Pb206/Pb204 (obs.)	Pb207/U235	±2σ (pct)	Pb206/U238	±2σ (pct)	Correl. Coeff. (rho)	Pb207/Pb206	±2σ (pct)	Pb206/U238 Age	±2σ (Ma)	Pb207/U235 Age	±2σ (Ma)	Pb207/Pb206 Age	±2σ (Ma)
Diorite																		
K-204	Zr-1	0.007	678	71	2067	0.8439	0.50	0.10123	0.48	0.956	0.06046	0.15	621.6	3.0	621.3	3.1	620.1	3.2
K-204	Zr-2	0.006	826	73	2676	0.6814	0.50	0.08226	0.48	0.969	0.06008	0.12	509.6	2.5	527.6	2.6	606.5	2.7
K-204	Zr-3	0.004	147	15	882	0.8945	1.10	0.10614	1.05	0.963	0.06112	0.30	650.3	6.8	648.8	7.1	643.4	6.3
Quartz–monzodiorite																		
K-104	Zr-1	0.007	508	52	1592	0.8250	0.59	0.09935	0.56	0.962	0.06023	0.16	610.6	3.4	610.8	3.6	611.8	3.5
K-104	Zr-2	0.003	1095	112	1651	0.8305	0.53	0.09998	0.51	0.972	0.06024	0.12	614.3	3.2	613.9	3.2	612.3	2.7
K-104	Zr-4	0.006	975	102	348	0.7439	0.53	0.08940	0.47	0.907	0.06035	0.22	552.0	2.6	564.7	3.0	616.0	4.8
K-104	Zr-3	0.006	306	34	1375	0.8451	0.57	0.10112	0.56	0.974	0.06061	0.13	621.0	3.5	621.9	3.6	625.6	2.8
K-104	Zr-5	0.010	377	42	1450	0.8482	0.51	0.10137	0.49	0.966	0.06068	0.13	622.5	3.1	623.7	3.2	628.0	2.8

Table 2
Rb–Sr isotopic whole-rock data.

		Rb (ppm)	Sr (ppm)	$^{87}Rb/^{86}Sr$	2σ	$^{87}Sr/^{86}Sr$	2σ	$(^{87}Sr/^{86}Sr)_i$	
								620 Ma	700 Ma
Diorite	K19	26.8	1037	0.0748	0.003	0.703953	0.000011	0.70329	0.70321
BHG	Fk12	144	539	0.7734	0.031	0.711422	0.000010	0.70458	0.70369
BHG	K34	163	427	1.1054	0.044	0.714176	0.000009	0.70440	0.70313
BHG	K35	139	468	0.8599	0.034	0.712336	0.000010	0.70473	0.70375
BHG	K70	145	488	0.8602	0.034	0.712058	0.000007	0.70445	0.70346
BHG	K75	121	598	0.5857	0.023	0.709946	0.000010	0.70476	0.70409
BHG	K56	170	685	0.7184	0.029	0.711223	0.000011	0.70487	0.70405
BmG	K61	242	211	3.3279	0.133	0.735137	0.000009	0.70571	0.70192
BmG	K68	349	175	5.7984	0.232	0.755678	0.000010	0.70440	0.69775
BmG	K72	271	383	2.0513	0.082	0.726040	0.000010	0.70790	0.70554
EsG	K52	175	717	0.7068	0.028	0.714603	0.000010	0.70835	0.70754
EsG	Ft3	177	745	0.6880	0.028	0.714558	0.000010	0.70847	0.70768
EsG	K51	129	285	1.3115	0.052	0.720339	0.000009	0.70847	0.70724
Amphibolites	AM1	60.5	746	0.2347	0.0094	0.706210	0.000008	0.70414	0.70386
Amphibolites	AM2	27.6	355	0.2246	0.0090	0.706710	0.000007	0.70472	0.70446
Amphibolites	K71	52.6	498	0.3059	0.0122	0.707609	0.000010	0.70490	0.70455

tionation corrected to $^{86}Sr/^{88}Sr = 0.1194$. Ages were calculated following Ludwig (2003). Results are given in Table 2.

Nd isotopes on whole rocks were measured at the Geowissenschaftliches Zentrum Göttingen-Isotopengeologie. Samples were spiked with a mixed $^{150}Nd/^{149}Nd$ Sm spike prior to dissolution. The separation was performed in two steps: cation exchange columns with HCl chemistry preceded a separation of Sm and Nd on Teflon columns coated with HDPE. The analyses were performed on a Finnigan MAT 262 TIMS operating in static mode. The total analytical error on the Sm and Nd abundances is <1%. The external reproducibility on a La Jolla standard solution was 0.511837 ± 0.000015. Nd compositions were corrected to a value of 0.511858 for the La Jolla standard and fractionation corrected to $^{146}Nd/^{144}Nd = 0.7219$. Single stage Nd model ages (T_{DM1}) were calculated according to the model of Michard et al. (1985) and Nelson and DePaolo (1985). Two-stage Nd model ages (T_{DM2}) were also calculated assuming a mean crustal $^{147}Sm/^{144}Nd$ ratio of 0.12 for the source prior to the intrusion age, using the evolving mantle curve of Nelson and DePaolo (1985). Results are given in Table 3.

5.2. Age results

Three zircons from one diorite (K204) and five zircons from one quartz–monzodiorite (K104), both from the BHG, were analyzed. The results are presented in Table 1 and Fig. 4. Two diorite zircons are concordant and one is discordant towards 0 Ma. The two concordant zircons give, respectively, 648 ± 5 Ma and 621 ± 3 Ma. This suggests an intrusion age for the diorite at 621 ± 3 Ma and an inherited zircon at 648 ± 5 Ma. Four zircons from the quartz–monzodiorite are concordant and one is discordant towards 0 Ma. Two zircons are concordant at 623 ± 2 Ma and the two others at 613 ± 2 Ma. This suggests an intrusion age for the quartz–monzodiorite at 613 ± 2 Ma with inherited zircons at 623 ± 2, possibly coming from the diorite: combining the magmatic zircon from the diorite with those zircons gives an age of 622 ± 4 Ma with an acceptable MSWD of 1.3. This suggests that the Fomopéa complex was emplaced within about 10 m.y. These U–Pb results on zircon indicate that the Fomopéa complex was emplaced at the end of the crustal thickening and represents an early generation of high-K calc-alkaline plutons emplaced in Cameroon, being older than most of the Pan-African plutons that intruded at ca. 580 Ma, during the second tectonic event. It is contemporaneous to the onset of the Yaoundé nappe tectonics towards the south (616–610 Ma; Toteu et al., 2006b).

Sixteen whole-rock Sr isotopes analyses were carried out and the results are presented in Table 2 and Fig. 5. The six samples from the biotite–hornblende granitoid define an isochron with an age of 572 ± 48 Ma (Sr initial ratio = 0.705520 ± 0.00053, MSWD = 1.15); the diorite is strongly below. The three samples from the biotite–monzogranite and the three from the edenite–syenogranite determine an isochron of 561 ± 34 Ma (Sr initial ratio = 0.70926 ± 0.00095, MSWD = 3.9). These ages are affected by large errors and partly based on mixed groups, which weaken

Table 3
Sm–Nd isotopic whole-rock data.

	Sm (ppm)	Nd (ppm)	$^{147}Sm/^{144}Nd$	2σ	$^{143}Nd/^{144}Nd$	2σ	εNd_0	$^{143}Nd/^{144}Nd$ (620 Ma)	εNd_{620}	T_{CHUR} (Ma)	T_{DM1} (Ma)	T_{DM2} (Ma)
Diorite												
K19	5.736	26.36	0.1316	0.0026	0.512563	0.000003	−1.5	0.512028	+4.04	176	923	898
BHG												
Fk12	6.17	25.3	0.1475	0.0029	0.512320	0.000004	−6.2	0.511721	−2.31	985	1613	1657
K34	6.75	30.5	0.1338	0.0027	0.512316	0.000006	−6.2	0.511776	−1.22	772	1364	1376
K35	8.00	31.4	0.1541	0.0031	0.512328	0.000004	−6.0	0.511702	−2.67	1108	1751	1821
K70	3.85	22.6	0.1030	0.0021	0.512291	0.000005	−6.8	0.511872	+0.66	565	1049	1038
K75	5.83	29.5	0.1195	0.0024	0.512325	0.000004	−6.1	0.511839	+0.01	619	1167	1162
K56	5.85	33.9	0.1044	0.0021	0.512253	0.000004	−7.5	0.511829	−0.19	636	1110	1103
BmG												
K61	4.28	27.3	0.0948	0.0019	0.511997	0.000008	−12.5	0.511612	−4.44	959	1332	1339
K68	3.73	21.5	0.1049	0.0021	0.512082	0.000004	−10.8	0.511656	−3.58	923	1337	1344
K72	4.38	32.8	0.0808	0.0016	0.511973	0.000003	−13.0	0.511645	−3.79	874	1226	1227
EsG												
K52	2.88	11.9	0.1463	0.0029	0.511623	0.000004	−19.8	0.511028	−15.83	3051	2976	3286
K51	2.40	11.8	0.1230	0.0025	0.512035	0.000007	−11.8	0.511535	−5.93	1246	1651	1689
Amphibolites												
AM1	6.72	38.62	0.1052	0.0021	0.512068	0.000025	−11.1	0.511558	−3.60	950	1358	1368
AM2	6.40	26.31	0.1471	0.0029	0.512499	0.000011	−2.7	0.511786	+1.60	428	1242	1244
K71	5.56	24.0	0.1398	0.0028	0.512343	0.000013	−5.7	0.511775	−1.25	791	1705	1444

T_{DM1} = single stage Nd model ages; T_{DM2} = two-stage Nd model ages.

the information. However, some conclusions can be given: (1) the Rb–Sr ages of the Fomopéa pluton are centred on the age of the right lateral wrench movements at 580 Ma that affected the complex and then also probably this isotopic system; (2) whatever this reactivation, different initial ratios are recorded following the facies considered with increasing Sr initial ratios with silica.

5.3. Nd–Sr isotopic characteristics

The $^{87}Sr/^{86}Sr$ initial ratios calculated at 620 Ma do not vary significantly within a given petrographical type: diorite (0.703), amphibolites (0.704), biotite–hornblende granitoid (0.704–0.705), biotite–monzogranite (0.704–0.708) and edenite–syenogranite (0.708–0.709). As for the Sr isotopes, the Nd isotopes are grouped when considering one petrographical type but show a large variation when the whole Fomopéa complex is considered: the diorite (K19) displays the most juvenile characteristics with moderately positive ε_{Nd} value (+4) and young T_{DM} (T_{DM1} = 0.90/0.92 Ga and T_{DM2} = 0.89 Ga). The BHG (Fk12, K34, K35, K70, K75, and K56) have ε_{Nd} around 0 (between +0.9 and −2.4) with T_{DM1} between 1.04 and 1.82 Ga and T_{DM2} between 1.03 and 1.82 Ga. The biotite monzogranite (K61, K68, and K72) have negative ε_{Nd} (between −3.3 and −4.2) with T_{DM1} between 1.23 and 1.34 Ga and T_{DM2} between 1.23 and 1.34 Ga. The edenite syenogranite has more crustal Nd signature. The two samples analyzed (K51 and K52) have more negative ε_{Nd} (−5.7 and −15.6) with older model ages T_{DM1} of 1.65 and 2.98 Ga and T_{DM2} 1.69 and 3.29 Ga. Palaeoproterozoic crust (2.1–1.66 Ga, U–Pb on zircon) is known in SW Cameroon (Penaye et al., 2004; Lerouge et al., 2006) and in Bafia region (Tchakounte et al., 2007) and Archaean crust (2.9 Ga, Rb–Sr isochron) in the nearby Congo craton (Lassere and Soba, 1976; Shang et al., 2004, 2007).

6. Geochemistry

6.1. Analytical procedures

Major and some trace elements were measured at the "Institut für Geowissenschaften, Christian-Albrechts-Universität zu Kiel,

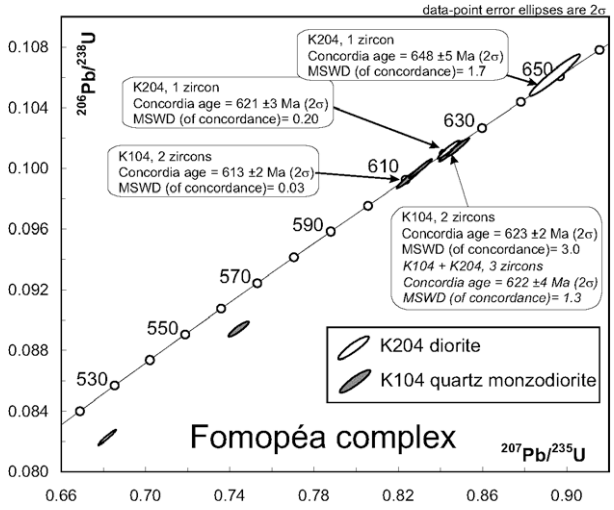

Fig. 4. Concordia diagram for the Fomopéa plutonic complex showing (a) quartz–monzodiorite and (b) diorite U–Pb ages.

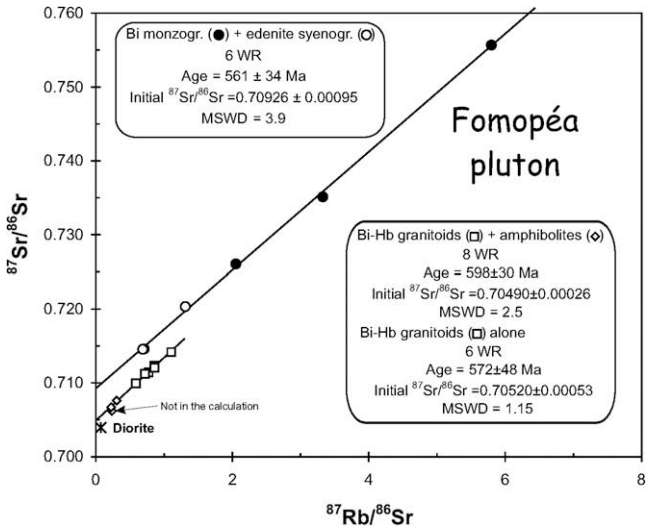

Fig. 5. Isochron Rb–Sr diagrams: (a) plot of BHG and (b) plot of BmG and EsG.

Table 4
Major (wt.%, recalculated to 100% on an anhydrous basis) and trace elements data for Fomopéa plutonic complex, n.m. and blank = not measured, b.d.l. = below detection limit.

	Amphibolites				Diorites				Biotite–hornblende granitoids (BHG)										
	K22	AM2	AM1	K71	K19	SO1	FK6	FK5	K1	K35	K45	K54	K75	FK12	K4	K34	K40	K56	K70
Major elements (recalculated for 100%)																			
SiO_2	51.55	50.12	56.79	50.37	51.78	52.55	51.78	49.06	63.39	64.39	61.35	65.63	62.85	63.35	66.65	69.42	72.99	68.96	66.57
TiO_2	0.80	2.11	1.11	1.05	1.52	1.70	1.63	1.38	0.71	0.65	0.90	0.63	0.75	0.69	0.66	0.40	0.20	0.59	0.49
Al_2O_3	14.07	14.22	16.46	11.85	19.03	16.71	20.13	18.71	14.93	15.56	16.61	15.14	15.30	16.40	14.97	14.38	13.91	15.16	15.17
Fe_2O_3	10.08	13.97	7.94	11.51	8.64	10.45	8.77	11.49	5.72	5.36	6.50	4.71	6.01	5.89	4.88	2.79	1.51	3.06	4.25
MnO	0.16	0.20	0.16	0.22	0.12	0.14	0.10	0.19	0.10	0.11	0.10	0.10	0.11	0.10	0.08	0.07	0.02	0.04	0.08
MgO	9.06	5.37	4.29	9.40	3.51	4.45	3.23	4.98	2.25	2.50	2.43	1.51	2.68	2.52	1.95	1.49	0.56	0.97	1.90
CaO	10.51	8.42	7.47	10.59	9.40	8.22	9.20	8.92	4.77	4.54	5.54	3.43	4.79	4.57	3.47	3.02	1.85	2.53	3.73
Na_2O	2.58	4.25	4.30	2.49	4.23	4.20	3.96	3.09	3.68	3.89	4.32	4.42	3.60	4.12	3.86	3.08	3.24	3.53	3.66
K_2O	1.18	1.05	1.12	1.11	1.08	1.26	0.87	1.69	3.31	3.52	1.75	4.09	3.21	2.73	3.73	4.99	5.40	4.92	3.72
P_2O_5	0.11	0.33	0.44	0.24	n.m	0.32	0.33	0.50	0.22	n.m	n.m	n.m	n.m	0.22	n.m	n.m	0.04	0.23	n.m
Total	100	100	100	100	100	100	100	100	100	100	100	100	100	100	100	100	100	100	100
LOI	0.23	n.m	n.m	0.50	0.70	n.m	n.m	n.m	0.51	0.45	0.49	0.28	0.6	0.35	0.5	0.31	0.29	0.53	0.41
$Na_2O + K_2O$	3.76	5.29	5.41	3.60	5.31	5.47	4.83	4.78	6.99	7.41	6.07	8.51	6.82	6.86	7.59	8.07	8.64	8.46	7.38
Mg/Mg + Fe	0.64	0.43	0.52	0.62	0.45	0.46	0.42	0.46	0.44	0.48	0.43	0.39	0.47	0.46	0.44	0.52	0.42	0.39	0.47
A/CNK	0.57	0.61	0.75	0.48	0.75	0.72	0.83	0.81	0.82	0.84	0.87	0.84	0.84	0.91	0.90	0.90	0.96	0.96	0.90
A/NK	2.55	1.75	1.99	2.24	2.34	2.02	2.70	2.71	1.55	1.53	1.84	1.29	1.63	1.68	1.44	1.37	1.24	1.36	1.51
$K_2O/CaO + Na_2O$ (molar)	0.09	0.08	0.09	0.09	0.08	0.09	0.06	0.14	0.34	0.36	0.16	0.43	0.34	0.27	0.42	0.69	0.83	0.66	0.43
Trace elements (ppm)																			
Li		7.7	n.m	n.m	35.9			35.4		39.6			58.4	39.5		14.4		26.8	33.5
Sc		42.5	n.m	n.m	80.2			66.2		55.6			35.9	54.6		46.1		40.5	35.3
Co		38.9	n.m	n.m	48.5			42.7		26.9			28	25.1		15.8		18.3	21.8
Ni		153.2	n.m	n.m	133			69.2		47.1			32.8	55		37.2		34.6	27.7
Cu		115.7	n.m	n.m	273			188		117			49	119		81.8		48.8	39.8
Zn		124.7	n.m	n.m	110			131		78.8			91.2	102		45.3		51.5	73.5
Ga		b.d.l.	n.m	n.m	31.1			29.2		26.4			27.9	27.3		21.5		23.5	25.3
Rb		25	28	53	34			96		145			139	150		174		170	157
Sr		328	355	498	1013			794		448			620	511		441		648	491
Y		37.2	16.9	18.3	22.9			36.2		23.1			36.3	18.6		26.6		18.5	18.2
Zr		174	173	110	153			85		178			181	173		99		181	173
Nb		8.5	12.3	8.5	12.7			9.80		16.90			14.8	14.3		20.9		20.8	13.1
Mo		n.m	n.m	n.m	4.2			2.5		2.4			2.0	2.7		4.2		2.9	1.5
Cs		n.m	n.m	n.m	4.4			6.5		11.9			9.4	14.3		4.3		5.9	7.8
Ba		208	557	265	466			671		635			867	443		889		1295	731
La		22.2	38.8	18.2	23.4			29.7		39.5			44.4	29.3		35.9		45.8	45.8
Ce		38.8	82.6	41.9	47.0			64.6		73.8			69.9	54.4		77.7		90	51.6
Pr		5.3	10.0	5.3	6.0			8.4		8.2			8.2	6.3		9.0		9.9	6.7
Nd		22.9	38.6	24.0	25.8			39.9		31.4			29.5	25.3		30.5		33.9	22.6
Sm		6.1	6.7	5.6	7.9			8.9		8			5.8	6.2		6.8		5.9	3.9
Eu		1.9	1.8	1.5	1.9			2.0		1.7			1.2	1.5		1.0		1.1	0.8
Gd		6.6	5.9	5.4	5.1			8.1		5.7			5.6	5.3		5.3		4.7	4.3
Tb		1.1	b.d.l.	b.d.l.	0.8			1.4		0.7			0.7	0.6		0.9		0.8	0.5
Dy		7.3	4.0	4.2	5.4			7.4		4.7			3.8	4.8		4.1		3.3	2.4
Ho		1.7	0.8	0.9	1.2			1.5		1.0			0.8	0.8		1.0		0.7	0.5
Er		4.4	2.2	2.3	3.0			3.6		2.0			2.6	2.6		3.0		1.9	1.4
Tm		0.6	b.d.l.	b.d.l.	0.6			0.7		0.4			0.3	0.4		0.6		0.4	0.3
Yb		3.8	1.8	2.0	4.0			3.3		2.3			2.0	2.5		3.1		1.8	1.7
Lu		0.6	0.3	0.3	0.5			0.6		0.5			0.3	0.4		0.5		0.4	0.3
Hf		4.2	3.8	2.9	3.9			3.4		5.7			4.8	5.5		3.4		5.2	4.7
Ta		0.4	0.7	0.4	1.0			0.8		1.3			0.8	1.3		1.9		2.2	0.8
Tl		0.2	b.d.l.	b.d.l.	0.7			0.8		0.9			0.6	1.4		1.2		1.0	0.7
Pb		4.2	11.2	8.3	35.4			15.0		25.3			18.3	25.8		33.8		29.2	25.7
Bi		b.d.l.	b.d.l.	b.d.l.	0.5			0.5		1.1			0.4	0.6		0.6		0.5	0.2
Th		2.0	4.6	5.5	4.1			2.9		18.2			11.2	18.1		45.6		38.6	30.4

U	0.9	1.0	2.8	1.3	1.2	7.4	3.6	8.0	7.5	3.9	7.3						
$(La/Yb)_N$	3.94	14.21	6.06	3.95	6.00	11.69	15.07	7.81	7.82	16.92	18.56						
$(La/Sm)_N$	2.25	3.56	2.01	1.83	2.05	3.05	4.70	2.93	3.28	4.83	7.34						
$(Gd/Yb)_N$	1.31	2.77	2.25	1.22	1.80	1.47	2.20	1.48	1.44	1.43	1.77						
Eu/Eu*	0.92	0.87	0.82	0.91	0.73	0.78	0.64	0.82	0.54	0.65	0.60						
ΣREE	123.16	193.49	111.37	132.30	180.05	179.94	175.08	140.44	179.20	200.56	142.83						

	Biotite monzogranites (BMG)										Edenite syenogranites (ESG)						
	K55	K13	K14	K61	K68	K58	K72	K74	MTO1	MTO2	K47	K50	K51	K52	FT3	FT4	FT50
Major elements (recalculated for 100%)																	
SiO_2	69.04	70.44	69.45	74.38	74.95	72.67	73.56	74.06	75.56	75.04	74.73	74.95	74.63	73.19	73.42	72.79	71.95
TiO_2	0.56	0.34	0.48	0.15	0.13	0.21	0.20	0.15	0.07	0.16	0.09	0.07	0.11	0.15	0.18	0.16	0.16
Al_2O_3	14.59	14.77	14.85	13.63	13.68	14.78	14.19	13.55	13.96	14.16	14.49	13.79	13.70	9.94	14.49	14.41	14.81
Fe_2O_3	3.00	2.58	2.91	1.21	0.94	1.47	1.48	1.17	0.62	1.14	0.98	0.91	0.94	1.68	1.48	1.59	1.56
MnO	0.05	0.02	0.04	0.02	0.02	0.02	0.02	0.04	0.01	0.04	0.02	0.03	0.01	0.05	0.04	0.03	0.05
MgO	1.22	0.61	0.78	0.19	0.14	0.10	0.22	0.18	0.00	0.40	0.03	0.03	0.38	0.39	0.13	0.35	0.40
CaO	2.61	1.59	1.92	1.32	0.99	1.13	1.26	1.05	0.72	0.97	0.87	0.89	1.31	1.14	1.05	1.03	1.14
Na_2O	3.59	2.94	2.89	3.32	3.74	3.40	3.41	3.41	4.30	3.49	4.21	4.85	4.88	4.52	4.11	4.61	4.78
K_2O	4.64	6.15	6.30	5.33	5.07	5.81	5.13	5.88	4.74	5.60	4.32	4.18	3.80	4.82	5.06	4.96	5.11
P_2O_5	n.m	n.m	n.m	n.m	n.m	0.05	n.m	0.03	0.01	0.03	0.01	n.m	n.m	n.m	0.03	0.06	0.05
Total	100	100	100	100	100	100	100	100	100	100	100	100	100	100	100	100	100
LOI	0.53	0.53	0.37	0.42	0.31	0.28	0.39	0.3	n.m	n.m	0.19	0.18	0.16	0.12	0.42	0.37	0.26
$Na_2O + K_2O$	8.23	9.09	9.20	8.65	8.81	9.21	8.55	9.29	9.04	9.09	8.53	9.03	8.68	9.34	9.17	9.52	9.83
Mg/Mg + Fe	0.45	0.32	0.35	0.24	0.23	0.12	0.23	0.24	0.00	0.41	0.06	0.06	0.44	0.32	0.15	0.31	0.34
A/CNK	0.93	1.03	0.99	1.00	1.02	1.06	1.05	0.98	1.03	1.04	1.10	0.98	0.94	0.67	1.02	0.97	0.96
A/NK	1.33	1.28	1.28	1.21	1.18	1.24	1.27	1.13	1.14	1.20	1.25	1.10	1.13	0.79	1.18	1.11	1.11
$K_2O/CaO + Na_2O$ (molar)	0.61	1.06	1.05	0.87	0.78	0.95	0.82	0.97	0.67	0.92	0.60	0.51	0.45	0.62	0.71	0.63	0.62
Trace elements (ppm)																	
Li				17.0	49.5		36.7				n.m		n.m	11.66		n.m	n.m
Sc				23.9	26.5		13.8				10		2	48.4		3	3
Co				7.4	6.8		4.9				7		n.m	13.4		2	2
Ni				13.6	17.2		9.6				n.m		n.m	38		n.m	110
Cu				27.7	30.9		15.3				30		n.m	88.8		n.m	n.m
Zn				39.8	43.7		64.9				60		n.m	42.5		n.m	n.m
Ga				28.0	31.6		30.5				13		15	22.7		16	15
Rb				256	366		310				144		109	178		178	162
Sr				211	173		395				1134		282	698		724	762
Y				12.1	11.3		7.4				32		12	12.9		18	13
Zr				146	121		202				207		64	113		122	124
Nb				14.5	15.2		9.0				12		6	10.8		8	7
Mo				0.8	1.1		0.4				n.m		n.m	1.0		n.m	n.m
Cs				6.5	9.9		6.5				1.6		b.d.l.	5.4		4.6	2.8
Ba				439	376		901				6721		344	1861		2007	2060
La				55.8	41.5		69.3				73.2		13.3	21.6		34.3	17.5
Ce				93.5	66.4		120				119		6.9	34.5		55.1	31
Pr				9.1	6.8		11.1				12.7		3.1	3.9		4.6	2.9
Nd				27.3	21.5		32.8				51.2		11.8	11.9		16	10.9
Sm				4.3	3.7		4.4				9.7		2.4	2.9		3	2.1
Eu				0.5	0.5		0.8				2.5		0.6	0.4		0.7	0.6
Gd				3.5	2.3		3.0				7.8		1.9	3.2		2.3	1.7
Tb				0.5	0.4		0.4				1.1		0.3	0.4		0.4	0.3
Dy				2.1	1.9		1.4				5.7		1.9	1.8		2.4	1.7
Ho				0.4	0.3		0.2				1.0		0.4	0.6		0.5	0.3
Er				1.3	1.2		0.7				3.0		1.2	1.5		1.5	1.1
Tm				0.2	0.2		0.1				0.5		0.2	0.3		0.2	0.2
Yb				1.3	1.1		0.4				2.7		1.3	1.4		1.5	1.1

(*continued on next page*)

Table 4 (*continued*)

	Biotite monzogranites (BMG)								Edenite syenogranites (ESG)					
	K55	K13	K14	K61	K68	K58	K72	K74	MTO1	MTO2	K47	K50	K51	K52	FT3	FT4	FT50
Lu				0.3	0.2		0.1				0.4		0.2	0.3		0.2	0.2
Hf				4.3	4.1		5.5				4.7		2.1	3.6		2.9	3.3
Ta				0.9	1.2		0.7				0.9		1.3	0.6		0.6	0.5
Tl				1.8	1.4		1.4				0.9		0.6	1.8		0.1	1.1
Pb				38.4	48.0		36.6				30.0		39.0	53.7		b.d.l.	45.0
Bi				0.1	0.1		0.1				b.d.l.		b.d.l.	0.4		b.d.l.	b.d.l.
Th				51.6	41.1		58.9				13.1		8.1	9.9		1.0	6.6
U				6.0	14.8		5.7				1.9		2.9	2.1		0.3	1.8
$(La/Yb)_N$				29.85	24.56		115.85				18.13		6.84	10.24		15.29	10.64
$(La/Sm)_N$				8.04	6.86		9.76				4.66		3.42	4.63		7.05	5.14
$(Gd/Yb)_N$				1.60	1.64		4.61				2.46		1.17	1.19		1.18	1.16
Eu/Eu*				0.40	0.55		0.64				0.88		0.81	0.35		0.82	0.89
ΣREE				200	148		244				290		45	85		123	72

n.m and blank = not measured; b.d.l. = below detection limit.

Germany" on fused discs by XRF technique. The 2σ-error for major elements is <1%, for trace elements <5%. All other trace elements were determined by ICP-MS, with errors $2\sigma < 20\%$ for Nb and Ta, <10% for Cs, Cu, Hf, Li, Ni, Sc, Y, Pb, Th, and U, and ≈5% for Rb, Sr, and the REE. Major elements have been recalculated to 100% without the loss of ignition (LOI) before use in the geochemical study. Representative data from 37 rock samples of three main groups from Fomopéa plutonic complex are given in Table 4.

6.2. Major elements

The SiO_2 contents range from 49 to 52.6 wt.% in diorites to 61.4% to 69.4 wt.% in the BHG and are higher and similar in the BmG (69.4–75.6 wt.%) and the EsG (71.9–75.0 wt.%). Harker diagrams (Fig. 6) show a general linear decrease in Al_2O_3, TiO_2, Fe_2O_3, CaO, and MgO with increasing SiO_2 at least for $SiO_2 > 60\%$. The diorites and the BHG belong to a calc-alkalic series while the BmG and the EsG belong to an alkali-calcic series (MALI diagram, Frost et al., 2001; Fig 7). This difference can be seen in the Na_2O vs. SiO_2 diagram (Fig. 6) where, with increasing SiO_2, Na_2O decreases in the BHG group and increases in the BmG group with opposite trends for K_2O (Fig. 8). In the total alkali–silica diagram ($Na_2O + K_2O$ vs. SiO_2), the three groups display a subalkaline affinity (Fig. 9a) whereas in the A/NK vs. A/CNK (Fig. 9b), BHG is metaluminous (A/CNK < 1), both EsG and BmG are metaluminous or weakly peraluminous (A/CNK = 0.94–1.1 with 2 samples > 1) except sample K52 from the EsG which is peralkaline (A/CNK: 0.67; NK/A: 1.22) due to a very low Al_2O_3 content. There is a silica gap (52–62%) between the diorites and the BHG and BmG, partly filled by an amphibolite. This rises to the relation existing between the granitoids. As we will see, the trace elements are similar all over the silica range, pointing to a common origin and a likely link trough a crystal fractionation process. Such a modelization would require more samples and is out of the scope of this study.

6.3. Trace and rare earth elements

The sliding normalization (each rock is normalized to the virtual rock from the reference series that has the same silica content) proposed by Liégeois et al. (1998) for distinguishing the potassic from the alkaline-peralkaline series confirms that no alkaline rocks are present in Fomopéa (Fig. 10). The Fomopéa rocks follow a potassic trend, parallel to the Y axis, implying a strong enrichment in LILE compared to HFSE. This diagram show that the EsG is not very rich in LILE if its silica content is taken into account, in agreement with the decrease in K_2O with SiO_2, due to the crystallization of K-rich minerals such as K-feldspar.

As a whole, trace elements (Fig. 11) are distributed non-uniformly in the three groups of rocks. The BHG group contains the highest content of Nb (20.9 ppm, lowest value – 6 ppm – in EsG), Y (36.3 ppm, lowest value – 7.4 ppm – in BmG), Hf (5.72 ppm, lowest value – 2.1 ppm – in EsG) and Ni (133 ppm, lowest value – 9.5 ppm – in BmG). The BmG group contains the highest contents of Rb (366 ppm, lowest value – 34 ppm – in BHG), Th (59 ppm, lowest value – 1 ppm – in EsG) and U (14.8 ppm, lowest value – 0.3 ppm – in EsG). The EsG group shows the highest content of Sr (1134 ppm, lowest value – 173 ppm – in BmG) and Zr (207 ppm, lowest value – 85 ppm – in BHG) and the highest and lowest content of Ba (6721 and 344 ppm); here, the samples with the highest Ba (K47) and lowest Ba (K51) also have the highest and lowest Sr and Zr contents of the group (Table 4). With the exception of those samples in the corresponding diagrams, rocks in the Harker diagrams behave differently from the group to another and sometimes within the same group with increasing SiO_2 (Fig. 11). Rb is incompatible in the BHG, dispersed in the BmG and shows a convex down profile in the EsG with a maximum (on-

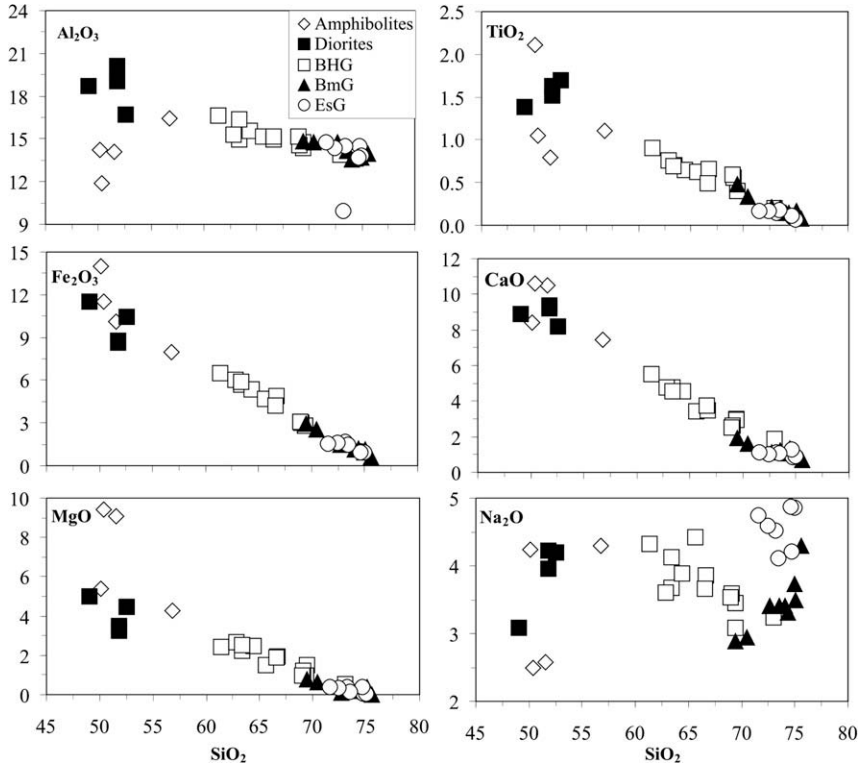

Fig. 6. Harker diagrams of selected major elements.

set of orthoclase crystallization) at 73.4 wt.% SiO_2. Ba, although dispersed, increases in the BHG and becomes compatible in the BmG and the EsG with steeper slope in the BmG. Sr decreases in the BHG in a dispersed way and remains compatible in the BmG and the EsG with similar slopes as for Ba. Zr is also compatible in the BmG and EsG, with a steeper slope in the BmG, whereas Nb displays three trends, each being incompatible, with steeper and parallel slopes in the BmG and EsG. The similar behaviour of Zr, Sr and Ba in the three remaining samples of EsG is also attested by their constant ratios (Sr/Zr = 5.93–6.18; Ba/Sr = 2.67–2.77; Ba/Zr = 16.45–16.61). Th is incompatible in BHG and EsG with more regular and steeper slope in BHG, and compatible in BmG. All these characteristics are compatible with a calc-alkalic source and a crystal fractionation process, low values of elements such as Nb or Th in the most evolved ESG facies being explained by the crystallization of late minerals uneasy to determine in the absence of the cumulates, generally formed in that case through filter-pressing (Hadj Kaddour et al., 1998).

REE contents are generally low in the Fomopéa rocks (45–290 ppm). The BmG has higher concentrations (148–243 ppm) followed by the BHG (132–201 ppm); the EsG have <123 ppm total REE with one sample (K47) at 290 ppm. The light rare earth elements are more enriched in the BmG (LREE/HREE: 18.6–38.5) than in the BHG (5.5–13.3) and the EsG (5.1–12.5). All rocks shows moderate negative europium anomalies excepted in amphibolites and diorites (Fig. 12): the negative Eu anomaly (Eu/Eu^*) is higher in the BmG (0.40–0.64) than in the EsG (0.80–0.89, with one sample at 0.35) and more variable in the BHG (0.60–0.91). The general patterns show LREE enrichment and almost flat HREE except in diorites. The Fomopéa REE patterns are similar to the Pan-African

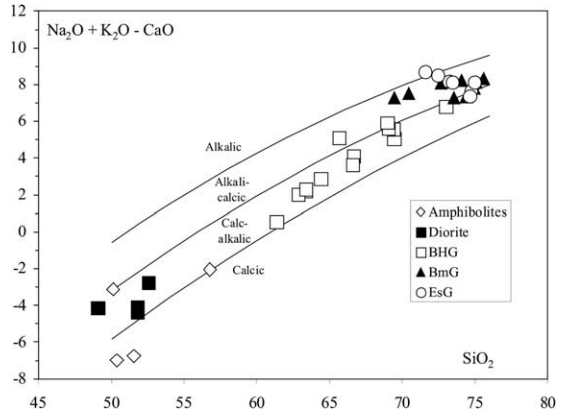

Fig. 7. MALI diagram from Frost et al. (2001). Plot of $Na_2O + K_2O - CaO$ vs. SiO_2 showing the ranges for the alkalic, alkali calcic, calc-alkalic, and calcic rock series. Fomopéa granitoids are calc-alkalic (diorites and BHG) and alkali-calcic (BmG and EsG).

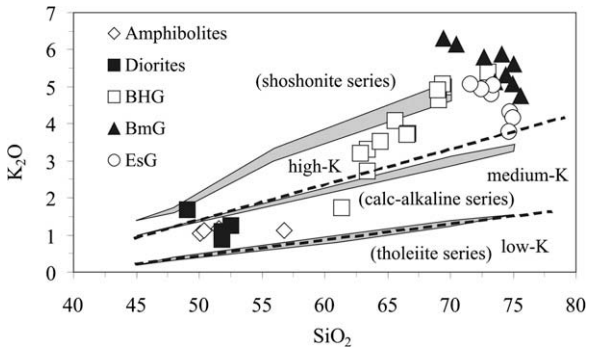

Fig. 8. Classification of the Fomopéa plutonic complex in the K_2O vs. Si_2O diagram. The diagram shows the subdivisions of Le Maitre et al. (2004) (broken lines) and of Rickwood (1989) (nomenclature in parentheses). The shaded bands are the fields in which the boundary lines of Peccerillo and Taylor (1976) are located.

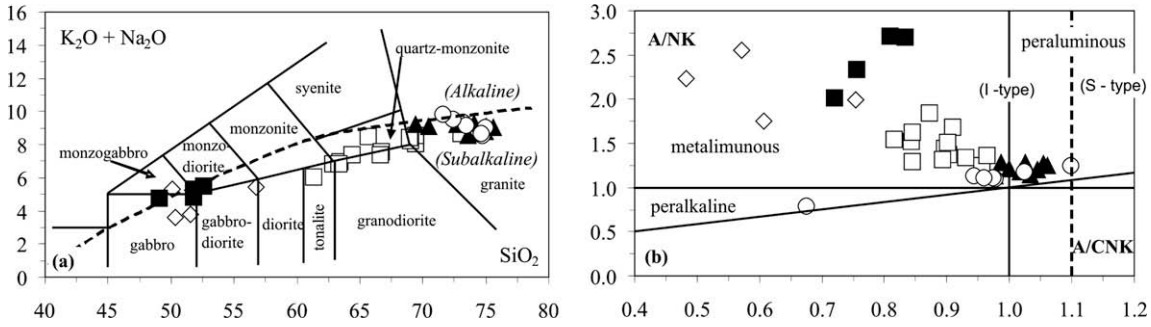

Fig. 9. (a) SiO_2 vs. $Na_2O + K_2O$ diagram, petrological subdivisions from Middlemost (1994); alkaline–subalkaline boundary line from Irvine and Baragar (1971). (b) Plot of the molecular ratio $Al_2O_3/(Na_2O + K_2O)$ vs. $Al_2O_3/(CaO + Na_2O + K_2O)$ after Maniar and Piccoli (1989).

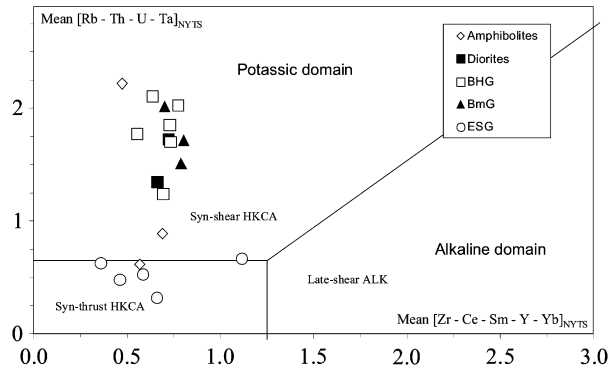

Fig. 10. Sliding normalization diagram comparing the Fomopéa plutonic complex to the reference syn-shear HKCA of the Yenchichi–Telabit series (Liégeois et al., 1998). The Fomopéa plutonic complex displays a strong potassic trend.

syn-shear granitic group from Aïr (Niger), sharing a similar geotectonic setting (Liégeois et al., 1998; Fig. 13). In spidergrams (Fig. 13), negative Nb, Ta and Ti anomalies are common and higher in the BmG and EsG than in the BHG. In addition, Th, Ce and P negative anomalies are common in the EsG, except in K47 for the Ce and in K51 for P which rather shows slight positive anomalies; Sr negative anomalies occur in the BmG; weak P negative anomalies are observed in the BHG and Zr negative anomalies occurs in diorites and some BHG samples. HREE enrichment relative to chondrite (Thompson, 1982) is higher in the BHG group than in the others. Globally, Fomopéa shows an enrichment of LILE over HFSE and Nb–Ta negative anomalies, both characteristics of high-K calc-alkaline or alkali-calcic series. This is shown with the similar patterns of the Aïr Pan-African syn-shear granitic group (Liégeois et al., 1998; Fig. 13).

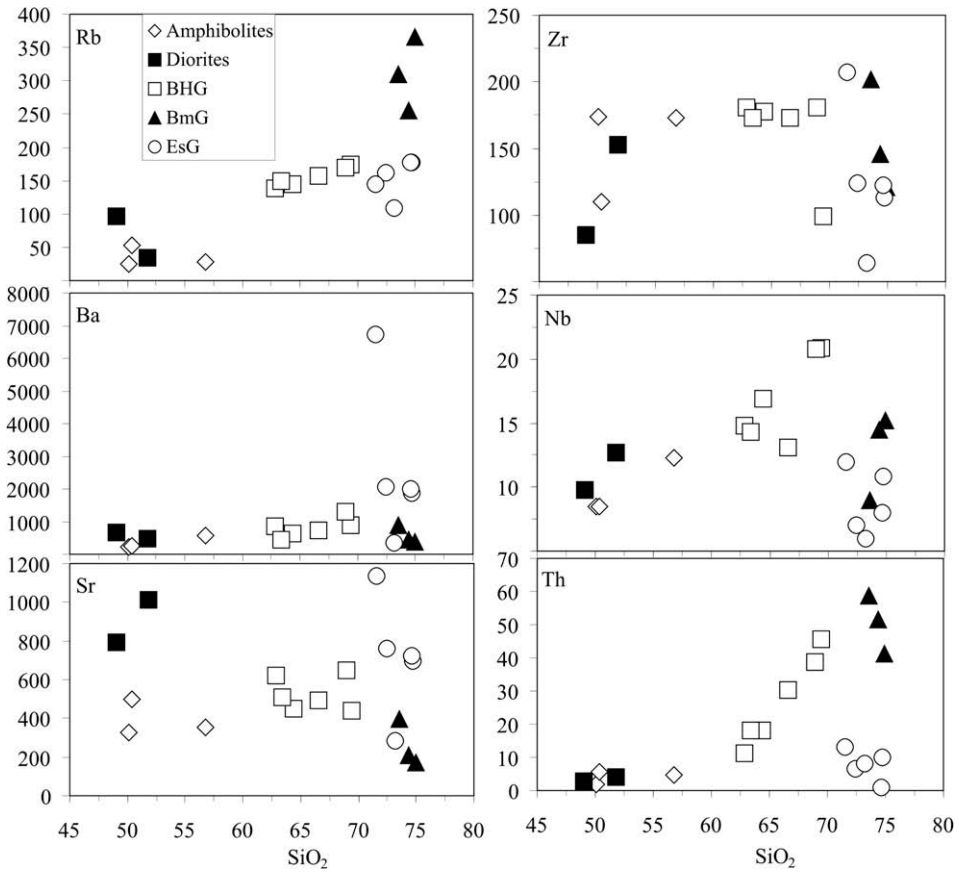

Fig. 11. Harker diagrams of selected trace elements.

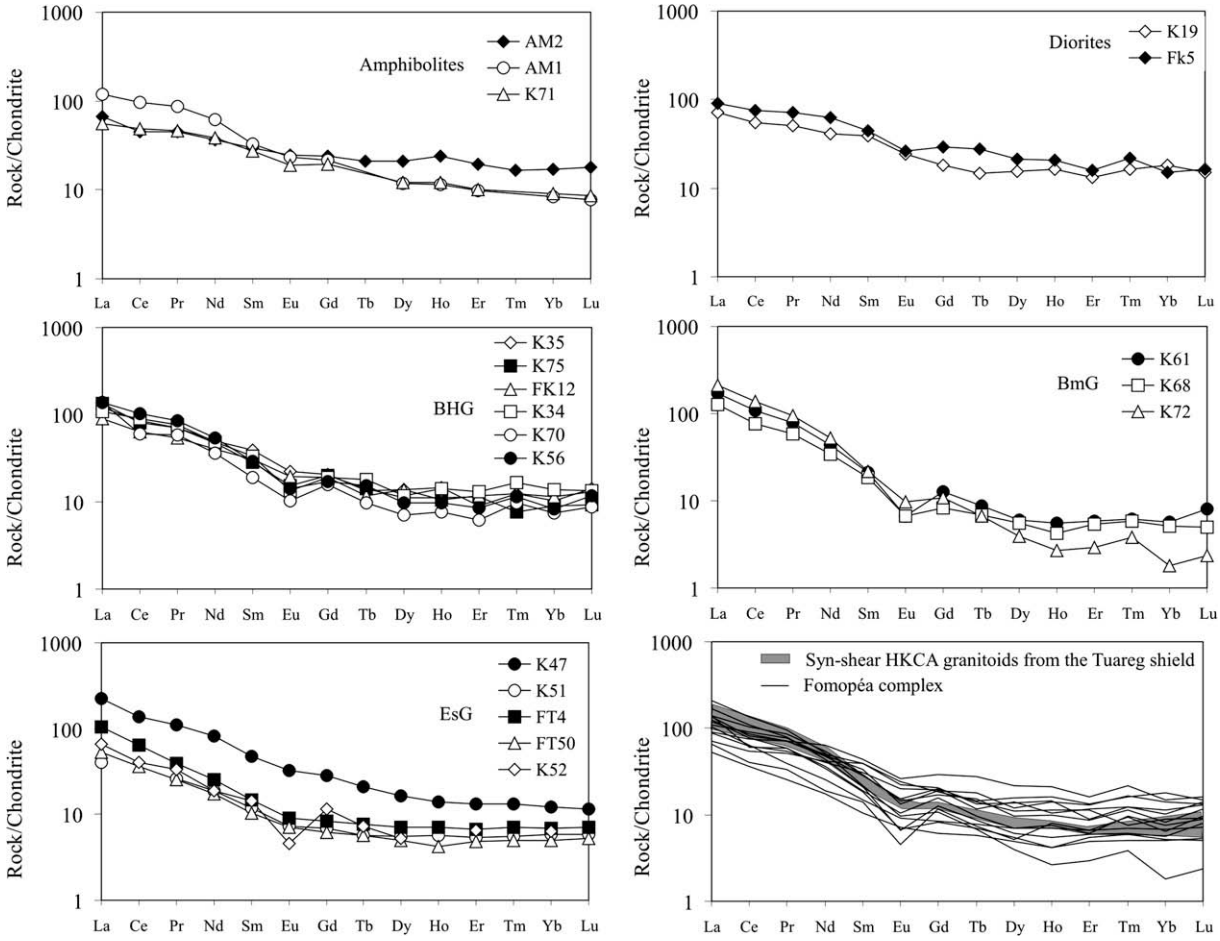

Fig. 12. Chondrite-normalized REE patterns for the Fomopéa plutonic complex. The normalizing values are from Nakamura (1974). Fomopéa complex rocks are compared to Adma and Iforas granitoids from syn-shear HKCA granitoids from the Tuareg shield (Liégeois et al., 1998).

7. Discussion

7.1. Nature and origin of the Fomopéa magmatism

The petrography, mineral chemistry and whole-rock geochemistry of the Fomopéa pluton are those of I-type calc-alkaline granitoids. More precisely, the calc-alkalic BHG rocks are similar to amphibole-rich calc-alkaline granitoids (ACG) and the alkali-calcic BmG and EsG rocks are comparable to K-rich and K-feldspar porphyritic calc-alkaline granitoids (KCG) of Barbarin (1999). Following the terminology of Sha and Chappell (1999), the BHG with its biotite and hornblende, SiO_2 contents between 60 and 69 wt.%, and ASI < 1, correspond to the mafic I-types, whereas the others, because of their higher SiO_2 contents and their metaluminous to weakly peraluminous compositions correspond to the felsic I-types.

According to Barbarin (1999), both the ACG and KCG are derived from mixing of mantle-derived basaltic magmas and crustal melts with varying proportions. The coexistence of mafic enclaves and gneissic country rocks in the Fomopéa plutonic complex indicates magma mixing on the one hand and interaction with the country rocks on the other hand. Th/La ratios suggest interaction between mantle and continental sources (Fig. 14).

Assessing the interaction between mantle and continental crust requires the use of Nd and Sr isotopes, recalculated to the age of intrusion (620 Ma). In the area of Fomopéa, the continental basement is represented by Eburnian (ca. 2 Ga) and Archaean rocks of the Congo craton and within the Yaoundé nappes. Part of this basement consists of Rb-depleted granulitic rocks. The Nd–Sr signature (Fig. 15) at 620 Ma of this basement is then in strong contrast with the mantle and there is no evidence for a juvenile continental crust at depth. The Fomopéa pluton displays a trend from a preponderantly mantle-derived signature represented by the diorites ($^{87}Sr/^{86}Sr$): 0.703, ε_{Nd} = +4, Nd T_{DM}: 0.9 Ga), towards the edenite syenogranite (EsG) displaying $^{87}Sr/^{86}Sr$ up to 0.7085, ε_{Nd} down to −15.8 and a Nd T_{DM} close to 3 Ga. The other samples lie between these two extremes (Fig. 14). This indicates a source combining an old felsic granulitic crust and a mafic mantle-derived magma (Fig. 15) probably at the origin of the heat needed for the crustal melting (Bonin, 2004). At 620 Ma, the most depleted mantle has $^{87}Sr/^{86}Sr$ = 0.70219 and ε_{Nd} = + 8.6. The diorites have a more enriched signature that can correspond either to such a depleted mantle with crust participation or to a more enriched mantle. The distinction between these two possibilities cannot be resolved here but whatever, the mantle signature in these rocks is largely preponderant. The felsic continental crust must include an Archaean segment for generating Archaean T_{DM}. A Palaeoproterozoic segment can have also participated as most of the T_{DM} ages are between 1 and 2 Ga. The close association of Archaean and Palaeoproterozoic rocks in the area supports such an interaction (Penaye et al., 2004; Tchakounte et al., 2007). This evidence thus links the Fomopéa magmatism with the continental crust melting generally evoked for other granitoids in the West Cameroon part of the Central Africa Pan-African fold belt, on the basis of their strong negative ε_{Nd} (e.g. the Ngondo complex, Tagne-Kamga, 2003; the Batoum granitoids, Nzolang et al., 2003 and Nzolang, 2005).

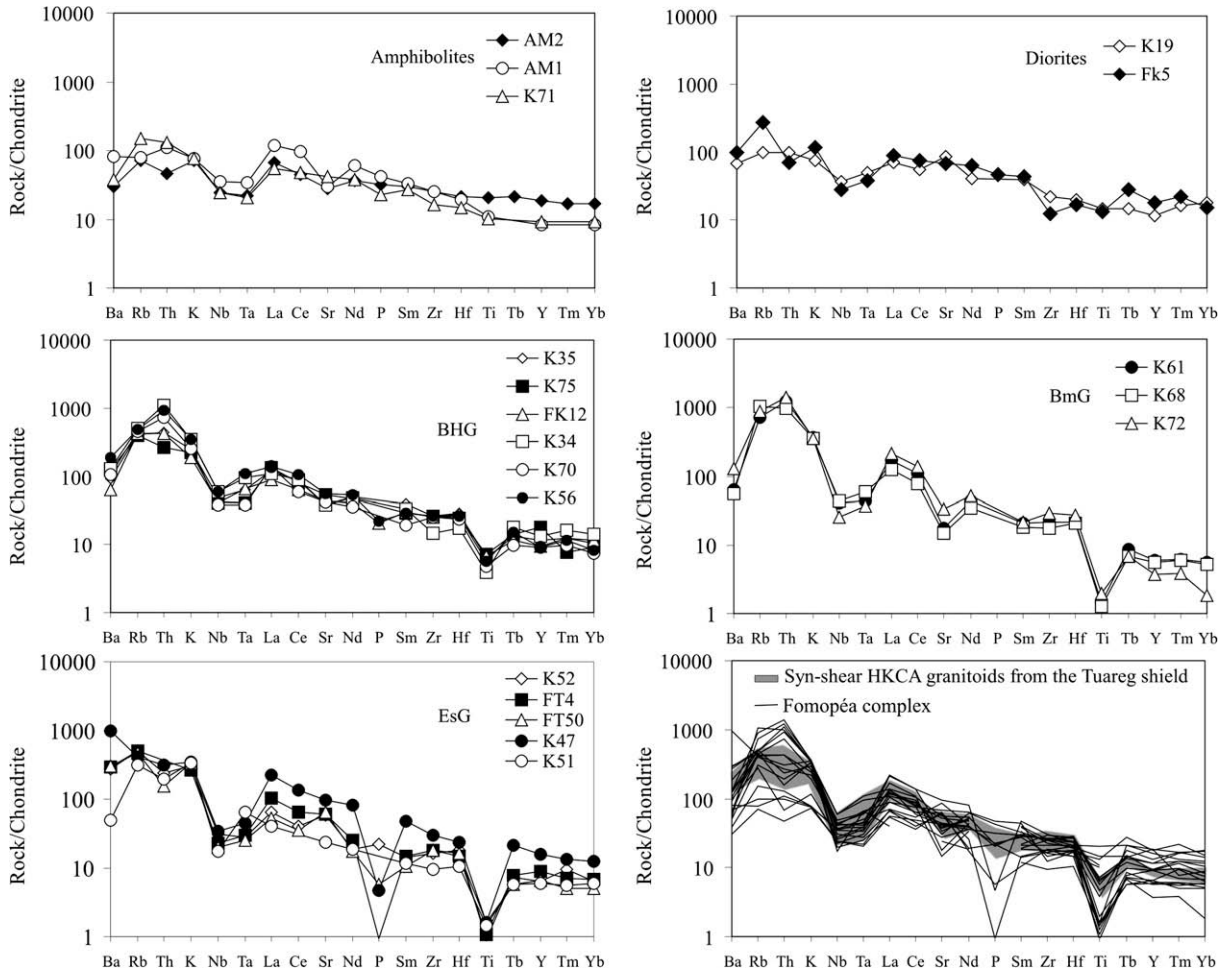

Fig. 13. Chondrite-normalized spidergrams using the normalization factors of Thompson (1982). Fomopéa complex rocks are compared to Adma and Iforas granitoids from syn-shear HKCA granitoids from the Tuareg shield (Liégeois et al., 1998).

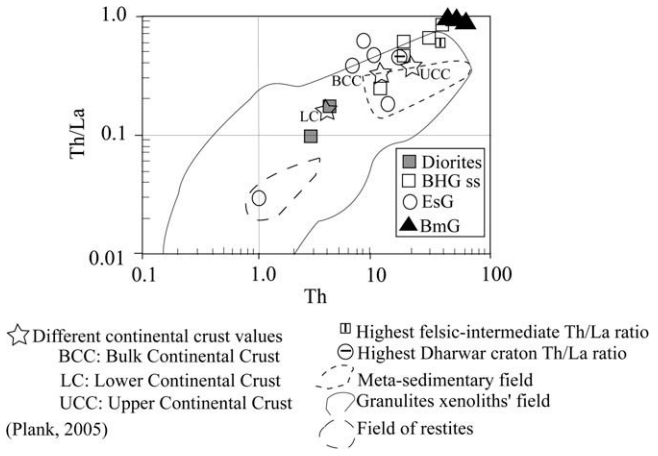

Fig. 14. Th vs. Th/La diagram from Plank (2005) showing the link between the different groups of Fomopéa rocks. Diorite sample occupies the array of mantle mafic rocks.

7.2. The Fomopéa plutonic complex and the evolution of the Cameroon Pan-African fold belt

The geochemical and mineralogical characteristics of granitoids are related to the nature of their protolith, as well as to the geodynamical environment under which their source magma formed and evolved (Roberts et al., 2000). The post-collisional environment is particularly rich in calc-alkalic and alkali-calcic granitoids originating from the remobilization of an older continental crust (Liégeois et al., 1998). The field relationships of the Fomopéa complex define its syn- to late kinematic emplacement relatively to the D_2 deformation. It is NE–SW elongated and has an emplacement age between 621 and 613 Ma (U–Pb ages) which corresponds to the end of crustal thickening in the area. The Fomopéa pluton has been affected by the right lateral wrench movements as shown by the Fomopéa Rb–Sr isochron reset to ca. 572 Ma. This tectonic event coincides with the emplacement of most of the post-collisional high-K calc-alkaline granitoids in the central domain of the Central Africa Pan-African fold belt (Nguiessi-Tchankam et al., 1997; Tagne-Kamga, 2003; Toteu et al., 2004, 2006a).

All these granites are intruded along the Central Cameroon Shear Zone (CCSZ; Fig. 1) and the parallel Sanaga Fault (SF; Fig. 1). To the south of the latter, the Pan-African Yaoundé nappes were thrust towards the Archaean craton. The Fomopéa pluton and its associated granitoids are located just to the north of an area characterized by a thick lithosphere as indicated by seismic tomography (Fig. 16). We can then suggest that the CCSZ and the SF mark the northern lithospheric boundary of the Congo craton and that the intrusion of these post-collisional granitoids is due to the post-collisional movements that occurred along this boundary. Such movements could occur during the start of a metacratonic evolution of the cratonic boundary, i.e. its fracturing by shear

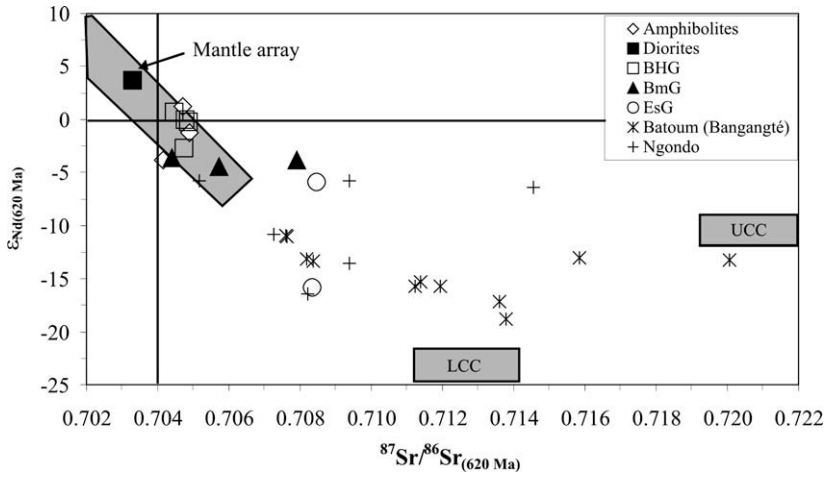

Fig. 15. $^{87}Sr/^{86}Sr_{620Ma}$ vs. $\varepsilon_{Nd620Ma}$ showing the evolution of the rocks from the Fomopéa plutonic complex, compared to the Batoum granitoids (Nzolang et al., 2003) and the Ngondo plutonic complex (Tagne-Kamga, 2003), which are mainly generated by crustal reworking. The Fomopéa plutonic complex defines a trend from the mantle array (diorites) towards an Archaean/Palaeoproterozoic continental crust, represented by both a Rb-depleted granulitic lower crust and a Rb-undepleted amphibolite upper crust.

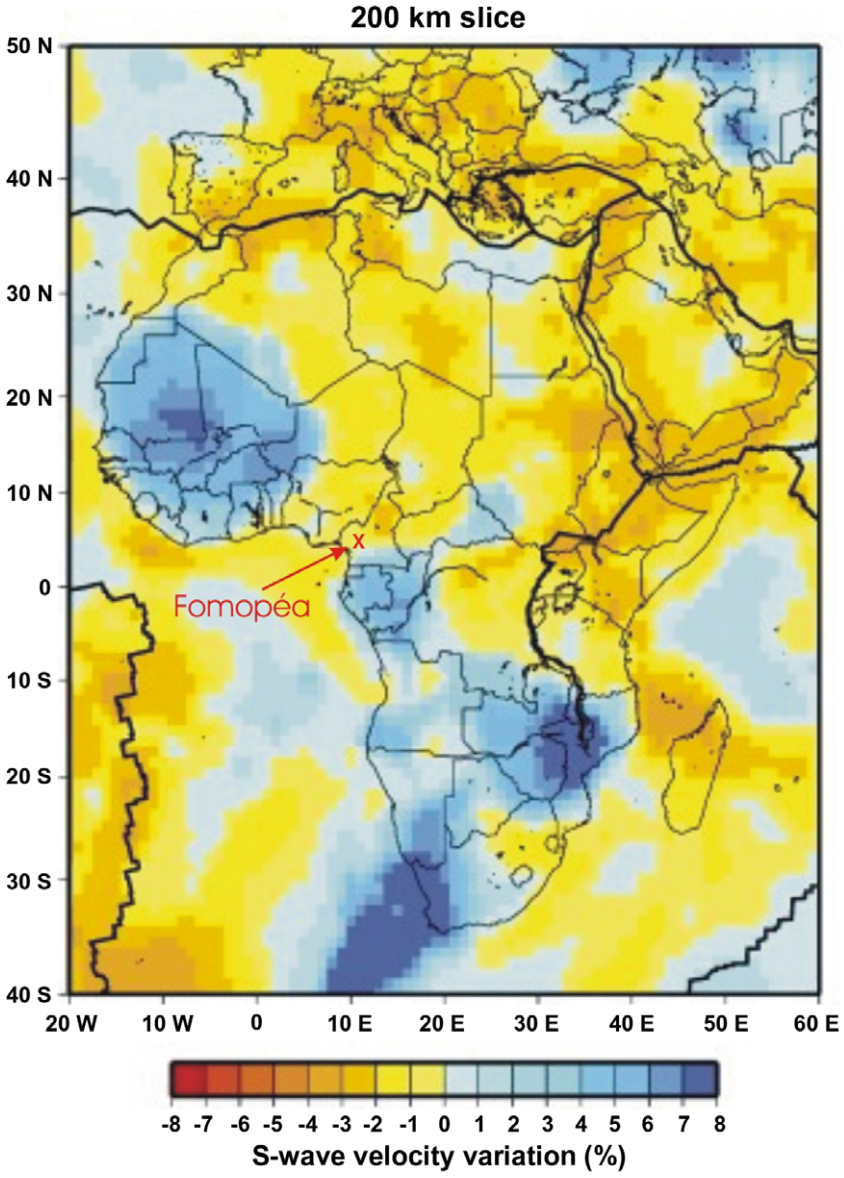

Fig. 16. Horizontal tomographical cross section of Africa showing the shear-wave velocity variation (in %) at 200 km depth (Pasyanos and Nyblade, 2007). This shows that the Fomopéa pluton is located along the northern boundary of the thick lithosphere of the Congo craton.

zones, invasion by mantle melts and the partial melting of the crust, but with the preservation of most of its cratonic rheology (Abdelsalam et al., 2002; Liégeois et al., 2003; Ennih and Liégeois, 2008). In such metacratonic areas, linear lithospheric delamination along mega-shear zones can occur, favouring the ascent of mantle-derived magmas and consequent crustal melting, giving rise to granitoids (Acef et al., 2003; Liégeois et al., 2003), similar to the Fomopéa pluton. The Fomopéa pluton would thus mark the onset of this stage. This metacratonization occurred during the convergence between the Congo craton and the Saharan metacraton (Abdelsalam et al., 2002). Other metacratonic boundaries rich in granitoids are known on the southern boundary of the Bangweulu craton (De Waele et al., 2006) and on the northern boundary of the West African craton (Ennih and Liégeois, 2008).

8. Conclusions

The Fomopéa plutonic complex is located at the south-western edge of the Central Cameroon mega Shear Zone (CCSZ). It comprises biotite–hornblende granitoids (BHG) associated with diorites and amphibolites, a biotite monzogranite (BmG) and an edenite syenogranite (EsG). The first rock types belong to a calc-alkalic series and the last two to an alkali-calcic series, all being I-type high-K calc-alkaline and metaluminous to weakly peraluminous.

The Fomopéa protolith corresponds to the Archaean and Palaeoproterozoic granulitic lower crust most probably that of the Congo craton melted by mantle-derived magmas, with mixed isotope ratios (Sr_{620} = 0.7030–0.7085 and ε_{Nd620} = −16 to +4 with T_{DM} model ages from 3 Ga to 0.9 Ga). Some relics of dismembered Palaeoproterozoic crust (2.1 Ga) are observed to the south of the Fomopéa area (Kékem granulites; Penaye et al., 2004).

We associate the origin of the Fomopéa pluton to the Pan-African convergence between the Congo craton and the Saharan metacraton that initiated the metacratonization of the northern boundary of the Congo craton. Post-collisional transpressive movements (strike-slip partitioned; Tagne-Kamga, 2003; Ngako et al., 2003) along the CCSZ (sinistral stage) and the SF induced linear lithospheric delamination allowing the uprise of mantle magmas (Black and Liégeois, 1993), triggering the partial melting of the old lower continental crust of the Congo craton's northern boundary. Mixing of the two types of magmas generated the Fomopéa pluton and the other Cameroon post-collisional granitoids. The Fomopéa pluton (621–613 Ma) corresponds to the initiation of the process (transition between crustal thickening and left lateral wrench movements), the climax being dated at ca. 580 Ma (late left lateral wrench movements to early right lateral wrench movements) during which most of the Cameroon granitoids intruded.

Acknowledgments

This study was performed during the stay of the first author in "Christian-Albrechts Universität Kiel" and "Geowissenschaftliches Zentrum Göttingen, Universität Göttingen" financed by the Germany Academic Exchange Organisation (DAAD). MK is grateful to Dietrich Ackermand of "Mineralogisches Institut, Universität Christian-Albrechts zu Kiel" and Gerhard Wörner of "Universität Göttingen" for their supervision. U- Pb data were carried in the project IGCP-470 by Sadrack Félix Toteu who is friendly acknowledged. Warm thanks are due to James Roberts and Abderrahmane Soulaimani for their detailed and thoughtful reviews that improved nicely this paper.

References

Abdelsalam, M.G., Liégeois, J.P., Stern, R.J., 2002. The Saharan metacraton. Journal African Earth Sciences 34, 119–136.

Acef, K., Liégeois, J.P., Ouabadi, A., Latouche, L., 2003. The Anfeg post-collisional Pan-African high-k calc-alkaline batholith (Central Hoggar, Algeria), result of the LATEA microcontinent metacratonization. Journal African Earth Sciences 37, 295–311.

Affaton, P., Rahaman, M.A., Trompette, R., Sougy, J., 1991. The Dahomeyide Orogen: tectonothermal evolution and relationships with the Volta Basin. In: Dallmeyer, R.D., Lécorché, J.P. (Eds.), The West African Orogens and Circum-Atlantic Correlatives. Springer-Verlag, Berlin, Heidelberg, pp. 107–122.

Almeida, F.F., Hasui, Y., Brito-Neves, B.B., Fuck, R.A., 1981. Brazalian structural provinces. Earth Sciences Review 17, 1–29.

Barbarin, B., 1999. A review of the relationships between granitoid types, their origins and their geodynamic environments. Lithos 46, 605–626.

Barbey, P., Macaudière, J., Nzenti, J.P., 1990. High-pressure dehydratation melting of the metapelites: evidences from the migmatites of Yaoundé (Cameroon). Journal of Petrology 31, 401–427.

Black, R., Liégeois, J.P., 1993. Cratons, Mobile belts, alkaline rocks and continental lithospheric mantle: the Pan-African testimony. Journal of the Geological Society of London 150, 89–98.

Bonin, B., 2004. Do coeval mafic and felsic magmas in post-collisional to within-plate regimes necessarily imply two contrasting, mantle and crustal, sources? A review. Lithos 78, 1–24.

Brito, Neves B.B., Van Schmus, W.R., Fetter, A., 2002. North-western Africa–North-eastern Brazil. Major tectonic links and correlation problems. Journal African Earth Sciences 34, 275–278.

De Waele, B., Liégeois, J.P., Nemchin, A.A., Tembo, F., 2006. Isotopic and geochemical evidence of Proterozoic episodic crustal reworking within the Irumide belt of South-Central Africa, the southern metacratonic boundary of an Archaean Bangweulu craton. Precambrian Research 148, 225–256.

Dumort, J.-C., 1968. Carte géologique de reconnaissance à l'échelle du 1/50000ième, République Fédérale du Cameroun, Notice explicative sur la feuille Douala-Ouest, Direction des Mines et de la Géologie du Cameroun.

Ekwueme, B.N., Caen-Vachette, M., Onyeagocha, A.C., 1991. Isotopic ages from the Oban Massif and southeast Lokoja: implications for the evolution of the basement complex of Nigeria. Journal African Earth Sciences 12, 489–503.

Ennih, N., Liégeois, J.P., 2008. The boundaries of the West African craton, with a special reference to the basement of the Moroccan metacratonic Anti-Atlas belt. In: Ennih, N., Liégeois, J.-P. (Eds.), The Boundaries of the West African Craton, vol. 298. Geological Society, London, pp. 1–17 (special publications).

Ferré, E., Caby, R., Peucat, J.J., Capdevila, R., Monié, P., 1998. Pan-African, post-collisional, ferro-potassic granite and quartz–monzonite plutons of Eastern Nigeria. Lithos 45, 255–279.

Ferré, E., Gleizes, G., Caby, R., 2002. Obliquely convergent tectonic and granite emplacement in the Trans-Sahara belt of Eastern Nigeria; a synthesis. Precambrian Research 114, 199–219.

Frost, B.R., Barnes, C.G., Collins, W.J., Arculus, R.J., Ellis, D.J., Frost, C.D., 2001. A geochemical classification for granitic rocks. Journal of Petrology 42, 2033–2048.

Ganwa, A., 1998. Contribution à l'étude géologique de la région de Kombé II-Mayabo dans la Série de Bafia: géomorphologie structurale, tectonique, pétrologie. Thèse Université Yaoundé I, 193 p.

Hadj Kaddour, Z., Liégeois, J.P., Demaiffe, D., Caby, R., 1998. The alkaline-peralkaline granitic post-collisional Tin Zebane dyke swarm (Pan-African Tuareg shield, Algeria): prevalent mantle signature and late agpaitic differentiation. Lithos 45, 223–243.

Johnson, M.C., Rutherford, M.J., 1989. Experimental calibration of the aluminium-in-hornblende geobarometer with application to Long Valley caldera (California) volcanic rocks. Geology 17, 837–841.

Irvine, T.N., Baragar, W.R.A., 1971. A guide to the chemical classification of the common volcanic rocks. Canadian Journal Earth Sciences 8, 523–548.

Krogh, T.E., 1982. Improved accuracy of U–Pb zircon ages by the creation of more concordant systems using an air abrasion technique. Geochimica Cosmochimica Acta 46, 637–649.

Kwékam, M., 1993. Le massif plutonique calco-alcalin pan-africain de Fomopéa (Ouest Cameroun), Cadre structural – Pétrologie – Géochimie, Interprétation géodynamique. Thèse 3ième Cycle Yaoundé I, 155 p.

Kwékam, M., 2005. Genèse et évolution des granitoïdes calco-alcalins au cours de la tectonique panafricaine: le cas des massifs syn à tardi-tectoniques de l'Ouest-Cameroun (Régions de Dschang et de Kekem). Thèse Etat, Université Yaoundé I, 194 p.

Lassere, M., Soba, D., 1976. Age cambrien des granites de Nybi et de Kongolo (centre-est Cameroun). Comptes Rendus Académie Sciences Paris 283, 1695–1698.

Le Maitre, R.W., Streckeisen, A., Zanettin, B., Le Bas, M.J., Bonin, B., Bateman, P., Bellieni, G., Dudek, A., Efremova, S., Keller, J., Lameyre, J., Sabine, P.A., Schmid, R., Sorensen, H., Woolley, A.R., 2004. Igneous Rocks, a Classification and Glossary of Terms. Cambridge University Press. 236 p..

Lerouge, C., Cocherie, A., Toteu, S.F., Penaye, J., Milési, J.P., Tchameni, R., Nsifa, E.N., Fanning, C.M., Deloule, E., 2006. Shrimp U–Pb zircon age evidence for Paleoproterozoic sedimentation and 2.05 Ga syntectonic plutonism in the Nyong group, South-Western Cameroon: consequences for the Eburnean-

Transamazonian belt of Ne Brazil and Central Africa. Journal African Earth Sciences 44, 413–427.
Liégeois, J.P., Navez, J., Hertogen, J., Black, R., 1998. Contrasting origin of post-collisional high-K calc-alkaline and shoshonitic versus alkaline and peralkaline granitoids. Lithos 45, 1–28.
Liégeois, J.P., Latouche, L., Boughara, M., Navez, J., Guiraud, M., 2003. The LATEA metacraton (Central Hoggar, Tuareg shield, Algeria): behaviour of an old passive margin during the Pan-African orogeny. Journal African Earth Sciences 37, 161–190.
Ludwig, K.R., 2003. Users manual for ISOPLOT/EX, version 3. A geochronological toolkit for Microsoft Excel. Berkeley Geochronology Center, Special Publication 4, 60 p.
Maniar, P.D., Piccoli, Ph.M., 1989. Tectonic discrimination of granitoids. Geological Society America Bulletin 101, 635–643.
Michard, A., Gurriet, P., Soudan, M., Albarède, F., 1985. Nd Isotopes in French Phanerozoic shales: external vs internal aspects of crustal evolution. Geochimica Cosmochimica Acta 49, 601–610.
Middlemost, E.A.K., 1994. Naming material in the magma/igneous rock system. Earth-Science Review 37, 215–224.
Nachit, H., Razafinahefa, N., Stussi, J.M., Caron, J.P., 1985. Composition chimique des biotites et typologie magmatique des granitoïdes. Comptes Rendus Académie Sciences Paris 301, 813–818.
Nakamura, N., 1974. Determination of REE, Ba, Fe, Mg, Na and K in carbonaceous and ordinary chondrites. Geochimica Cosmochimica Acta 38, 757–775.
Nédélec, A., Macaudière, J., Nzenti, J.P., Barbey, P., 1986. Evolution structurale et métamorphique des schistes de Mbalmayo (Cameroun). Implications sur la structure de la zone mobile panafricaine d'Afrique Centrale au contact du craton du Congo. Comptes Rendus Académie Sciences Paris 303, 75–80.
Nelson, B.K., DePaolo, D.J., 1985. Rapid production of continental crust 1.7 to 1.9 b.y. ago: Nd isotopic evidence from the basement of the North American mid-continent. Geological Society American Bulletin 96, 746–754.
Ngako, V., 1986. Evolution métamorphique et structurale de la bordure Sud-Ouest de la "Série de Poli" (segment camerounais de la chaîne panafricaine). Mémoires et documents du Centre armoricain d'étude structurale des socles 5, 185 p.
Ngako, V., 1999. Les déformations continentales panafricaines en Afrique centrale, résultat d'un poinçonnement de type himalayen. Thèse Doctorat Etat, Université Yaoundé I, 301 p.
Ngako, V., Jégouzo, P., Nzenti, J.P., 1991. Le cisaillement centre camerounais. Rôle structural et géodynamique dans l'orogenèse panafricaine. Compte Rendus Académie Sciences Paris 313, 457–463.
Ngako, V., Jégouzo, P., Nzenti, J.P., 1992. Champ de raccourcissement et cratonisation du Nord Cameroun du Protérozoïque supérieur au Paléozoïque moyen. Comptes Rendus Académie Sciences Paris 315, 371–377.
Ngako, V., Affaton, P., Nnange, J.M., Njanko, Th., 2003. Pan-African tectonic evolution in central and southern Cameroon: transpression and transtension during sinistral shear movements. Journal African Earth Sciences 36, 207–214.
Ngako, V., Affaton, P., Njonfang, E., 2008. Pan-African tectonics in northwestern Cameroon: implication for the history of western Gondwana. Gondwana Research 14, 509–522.
Nguiessi-Tchankam, Cl., Nzenti, J.P., Nsifa, E.N., Tempier, P., Tchoua, F., 1997. A calc-alkaline magmatic complex from Bandja in the north-equatorial fold belt; a synkinematic emplacement of plutonic rocks in a sinistral strike-slip shear zone from Pan-African age. Comptes Rendus Académie Sciences Paris 325, 95–101.
Njel, U.O., 1986. Paléogéographie d'un segment de l'orogène panafricain, la ceinture volcano-sédimentaire de Poli (Nord-Cameroun). Comptes Rendus Académie Sciences Paris 303, 1737–1742.
Njonfang, E., 1998. Contribution à l'étude de la relation entre la "Ligne du Cameroun" et la direction de l'Adamoua: 1 – pétrologie, géochimie et structure des granitoïdes panafricains de la zone de cisaillement Foumban-Bankim (Ouest-Cameroun); 2 – pétrologie et géochimie des formations magmatiques tertiaires associées. Thèse Etat Université Yaoundé I, 392 p.
Njonfang, E., Ngako, V., Kwékam, M., Affaton, P., 2006. Les orthogneiss calco-alcalins de Foumban-Bankim: témoins d'une zone de cisaillement de haute température. Comptes Rendus Geosciences 338, 606–616.
Njonfang, E., Ngako, V., Moreau, C., Affaton, P., Diot, H., 2008. Restraining bends in high temperature shear zone: the "Central Cameroon Shear Zone", Central Africa. Journal African Earth Sciences 52, 9–20.
Nzolang, C., 2005. Crustal evolution of the Precambrian basement in west Cameroon: inference from geochemistry, Sr–Nd isotopes and experimental investigation of some granitoids and metamorphic rocks. Ph.D. thesis Niigata University, Japan, 207 p.
Nzolang, C., Kagami, H., Nzenti, J.P., Holtz, F., 2003. Geochemistry and preliminary Sr–Nd isotopic data on the Neoproterozoic granitoids from the Bantoum area, West Cameroon: evidence for a derivation from a Paleoproterozoic to Archean crust. Polar Geoscience 16, 196–226.
Pasyanos, M.E., Nyblade, A.A., 2007. A top to bottom lithospheric study of Africa and Arabia. Tectonophysics 444, 27–44.
Peccerillo, A., Taylor, S.R., 1976. Geochemistry of Eocene calc-alkaline volcanic rocks from the Kastamonu area, Northern Turkey. Contribution Mineralogy Petrology 58, 63–81.
Penaye, J., Toteu, S.F., Van Schmus, W.R., Nzenti, J.P., 1993. U–Pb and Sm–Nd preliminary geochronologic data on the Yaoundé series, Cameroon: re-interpretation of the granulitic rocks as the suture of a collision in the "Centrafrican belt". Comptes Rendus Académie Sciences Paris 317, 789–794.
Penaye, J., Toteu, S.F., Tchameni, R., Van Schmus, W.R., Tchakounté, J., Ganwa, A., Minyem, D., Nsifa, E.N., 2004. The 2.1 Ga West Central African belt in Cameroon. Journal African Earth Sciences 39, 159–164.
Plank, T., 2005. Constraints from thorium/lanthanum on sediment recycling at subduction zones and the evolution of the continents. Journal of Petrology 46, 921–944.
Rickwood, P.C., 1989. Boundary lines within petrologic diagrams which use oxides of major and minor elements. Lithos 22, 247–263.
Roberts, M.P., Pin, C., Clemens, J.D., Paquette, J.L., 2000. Petrogenesis of mafic to felsic plutonic rock associations: the calc-alkaline Quérigut Complex, French Pyrénées. Journal of Petrology 41, 809–844.
Sha, L.-K., Chappell, B.W., 1999. Apatite chemical composition, determined by electron microprobe and laser-ablation inductively coupled plasma mass spectrometry, as a probe into granite petrogenesis. Geochimica Cosmochimica Acta 63, 3861–3881.
Shang, C.K., Satir, M., Siebel, W., Nsifa, E.N., Taubald, H., Liégeois, J.P., Tchoua, F.M., 2004. TTG magmatism in the Congo craton; a view from major and trace element geochemistry, Rb–Sr and Sm–Nd systematics: case of the Sangmelima region, Ntem complex, southern Cameroon. Journal African Earth Sciences 40, 61–79.
Shang, C.K., Satir, M., Nsifa, E.N., Liegeois, J.P., Siebel, W., Taubald, H., 2007. Archaean high-K granitoids produced by remelting of earlier Tonalite–Trondhjemite–Granodiorite (TTG) in the Sangmelima region of the Ntem Complex of the Congo craton, southern Cameroon. International Journal Earth Sciences 96, 817–841.
Soba, D., Michard, A., Toteu, S.F., Norman, D.I., Penaye, J., Ngako, V., Nzenti, J.P., Dautel, D., 1991. Données géochronologiques nouvelles (Rb–Sr, U–Pb et Sm–Nd) sur la zone mobile panafricaine de l'Est Cameroun: âge Protérozoïque supérieur de la série de Lom. Comptes Rendus Académie Sciences Paris 312, 1453–1458.
Tagne-Kamga, G., 2003. Petrogenesis of the Neoproterozoic Ngondo plutonic complex West Cameroon Central Africa): a case of late-collisional ferro-potassic magmatism. Journal African Earth Sciences 36, 149–171.
Talla, V., 1995. Le massif granitique panafricain de Batié (Ouest Cameroun); Pétrologie-Pétrostructurale-Géochimie. Thèse 3ième Cycle, Université Yaoundé I, 144 p.
Tchakounté, J., 1999. Etude géologique de la région d'Etoundou-Bayomen dans la série de Bafia (province du Centre): tectonique, géochimie-métamorphisme. Thèse Université Yaoundé I, 190 p.
Tchakounte, J., Toteu, S.F., Van Schmus, W.R., Penaye, J., Deloule, E., Mvondo Ondoua, J., Bouyo Houketchang, M., Ganwa, A.A., White, W.M., 2007. Evidence of ca 1.6-Ga detrital zircon in the Bafia Group (Cameroon): implication for the chronostratigraphy of the Pan-African Belt north of the Congo craton. Comptes Rendus Geoscience 339, 132–142.
Tchouankoué, J.P., 1992. La syénite de Bangangté: un complexe pan-africain à caractères intermédiaires. Pétrologie-géochimie. Thèse 3ième Cycle Université Yaoundé, 161 p.
Thompson, R.N., 1982. Magmatism of the British Tertiary province. Scottish Journal Geology 18, 49–107.
Toteu, S.F., 1990. Geochemical characterization of the main petrographical and structural units of northern Cameroon: implications for the Pan-African evolution. Journal African Earth Sciences 10, 615–624.
Toteu, S.F., Michard, A., Bertrand, J.M., Rocci, G., 1987. U/Pb dating of Precambrian rocks from Northern Cameroon, orogenic evolution and chronology of the Pan-African belt of Central Africa. Precambrian Research 37, 74–87.
Toteu, S.F., Macaudière, J., Bertrand, J.M., Dautel, D., 1990. Metamorphic zircons from North-Cameroon: implications for the Pan-African evolution of Central Africa. Geologische Rundschau 79, 777–788.
Toteu, S.F., Van Schmus, R.W., Penaye, J., Nyobe, J.B., 1994. U–Pb and Sm–Nd evidence for Eburnian and Pan-African high-grade metamorphism in cratonic rocks of southern Cameroon. Precambrian Research 67, 321–347.
Toteu, S.F., Van Schmus, R.W., Penaye, J., Michard, A., 2001. New U–Pb and Sm–Nd data from North-Central Cameroon and its bearing on the pre-Pan African history of Central Africa. Precambrian Research 108, 45–73.
Toteu, S.F., Penaye, J., Djomani, Y.P., 2004. Geodynamic evolution of the Pan-African belt in Central Africa with special reference to Cameroon. Canada Journal Earth Sciences 41, 73–85.
Toteu, S.F., Penaye, J., Deloule, E., Van Schmus, W.R., Tchameni, R., 2006a. Diachronous evolution of volcanosedimentary basins north of the Congo craton: insights from U–Pb ion microprobe dating of zircons from the Poli, Lom and Yaoundé Groups (Cameroon). Journal African Earth Sciences 44, 428–442.
Toteu, S.F., Yongue Fouateu, R., Penaye, J., Tchakounte, J., Seme Mouangue, A.C., Van Schmus, W.R., Deloule, E., Stendal, H., 2006b. U–Pb dating of plutonic rocks involved in the nappe tectonic in southern Cameroon: consequence for the Pan-African orogenic evolution of the Central African fold belt. Journal African Earth Sciences 44, 479–493.
Tubosum, I.A., 1983. Géochronologie U–Pb du socle précambrien du Nigéria. Thèse 3ième Cycle Université Montpellier, 144 p.